

Autonomous Cooperative Wall Building by a Team of Unmanned Aerial Vehicles in the MBZIRC 2020 Competition

Tomas Baca^{a,1,c}, Robert Penicka^{a,c}, Petr Stepan^{a,c}, Matej Petrlik^a, Vojtech Spurny^a, Daniel Hert^a, Martin Saska^a

^aAuthors are with the Faculty of Electrical Engineering, Czech Technical University in Prague, Technicka 2, Prague 160 00.

^bCorresponding author, e-mail: tomas.baca@fel.cvut.cz.

^cAuthors contributed equally.

Abstract

This paper presents a system for autonomous cooperative wall building with a team of Unmanned Aerial Vehicles (UAVs). The system was developed for Challenge 2 of the Mohamed Bin Zayed International Robotics Challenge (MBZIRC) 2020. The wall building scenario of Challenge 2 featured an initial stack of bricks and wall structure where the individual bricks had to be placed by a team of three UAVs. The objective of the task was to maximize collected points for placing the bricks within the restricted construction time while following the prescribed wall pattern. The proposed approach uses initial scanning to find a priori unknown locations of the bricks and the wall structure. Each UAV is then assigned to individual bricks and wall placing locations and further perform grasping and placement using onboard resources only. The developed system consists of methods for scanning a given area, RGB-D detection of bricks and wall placement locations, precise grasping and placing of bricks, and coordination of multiple UAVs. The paper describes the overall system, individual components, experimental verification in demanding outdoor conditions, the achieved results in the competition, and lessons learned. The presented CTU-UPenn-NYU approach achieved the overall best performance among all participants to win the MBZIRC competition by collecting the highest number of points by correct placement of a high number of bricks.

1. Introduction

UAVs belong to one of the most studied topics in the field of robotics due to the numerous possible applications. One of the possible areas of the UAV deployment is in construction [1] where the UAVs can, for example, visually inspect existing construction sites, survey areas before construction starts, or monitor security and safety of the sites [2, 3]. This paper goes beyond these works to present a fully autonomous system enabling physical interaction and not only inspection. The UAVs directly take part in the construction and are used for building walls. The proposed multi-robot system is designed in order to autonomously build walls with only a little a priori knowledge of the construction site. The system uses onboard detection of bricks and wall structure locations using carried camera and depth sensors. An initial scan of the construction area is conducted using one UAV to find the locations of the brick stack and of the wall building site. Afterwards, each UAV is assigned to a particular stack part and wall segment to then cooperatively build the wall according to a given wall pattern. During the building process, each UAV repeatedly attempts to grasp a brick from the assigned stack, delivers the brick above the designated segment of the wall, and then precisely places the brick on the wall. Figure 1 illustrates the scanning, grasping, and placing subtasks of the wall building.

The proposed system was developed by the joint CTU-UPenn-NYU¹ team for the participation in Challenge 2 of the

MBZIRC 2020 [4]. Challenge 2 consisted of the wall building task where three UAVs and one Unmanned Ground Vehicle (UGV) were assigned to autonomously build two walls — one by the UGV and one by the UAVs. This paper presents details of the system used for the UAV part of the challenge. The challenge featured brick stacking for the UAVs containing 46 bricks, each with ferromagnetic plate on top to facilitate grasping. Four types of bricks were present, each with different color, weight, length, and earned points for placement. The future wall structure for the UAVs consisted of four segments arranged in a ‘W’ letter shape located 1.7 m above ground, capable of containing all the bricks from the stack in only two layers. The goal of the challenge was to maximize collecting points by autonomously placing the bricks on the wall according to a given wall pattern in a given time limit.

The wall building approach by the CTU-UPenn-NYU team exhibited the best performance among all participants of the MBZIRC 2020 Challenge 2. During the two competition trials, each with a duration of 25 minutes, the UAVs were able to grasp a total number of 17 bricks and successfully place ten of them. The UGV helped by placing one brick to fulfill the requirements for winning the challenge. The CTU-UPenn-NYU team was thus able to place the most bricks among the participants to achieve a score of 8.24- far higher than the second best team with a score of 1.33 points.

The solution proposed for the wall building task consists of three main autonomous capabilities of the UAVs. The first is

¹Collaboration of the Czech Technical University in Prague, University of

Pennsylvania, and New York University.

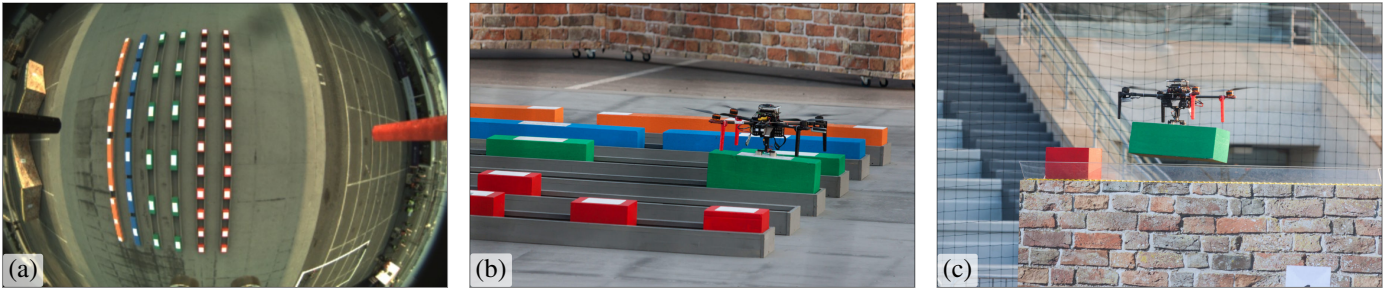


Figure 1: Illustration of the proposed UAV system for the wall building task showing images captured from the onboard camera during scanning (a) and photos of UAV during brick grasping (b) and placing (c).

the scanning of the arena to find locations of the brick stack and the wall. All detections from the one UAV performing the scanning are used to create a topological map of the arena which is created by employing statistical analysis of the detections using known sizes and shapes of the brick stack and the wall segments. Distribution of the wall building task is then based on sharing the topological map among the UAVs using Wi-Fi communication and deterministic assignment of the brick stack and wall parts to individual UAVs. Each UAV then creates a plan to grasp and place according to a given wall pattern and assigned part, and afterward repeats grasping and placing until battery depletion or plan fulfillment.

The second primary capability is for brick grasping, which requires precise navigation of the UAV to the center of the brick marked by a white ferromagnetic plate. The most essential part of ensuring precise grasping is robust and fast brick detection. The color and Red-Green-Blue-Depth (RGB-D) cameras provide sufficient information about brick position from altitudes above the bricks and their fusion improves the robustness of detection. The duration of brick detection for grasping was no longer than 7 ms and thus allowed the use of a visual servoing technique during the final approach to increase grasping precision. A grasping state machine is used to govern various stages of approaching the brick, e.g., decides when to switch from Global Positioning System (GPS) localization to visual servoing. Finally, both the UAV estimated mass and attitude are checked during grasping by the UAV control system to abort grasping in close brick interactions when, e.g., the brick is grasped far from the center of mass or the UAV mass is transferred to the ground by its landing gear.

The last main autonomous capability is the placement of a brick to a desired position on the wall structure. This task is challenging as the grasped brick may influence wall detection due to the sensors possibly being obscured by the brick. The brick may further influence the UAV control system as additional brick mass could generate torque to the UAV if not grasped exactly above the center of mass. The brick concealing a significant amount both sensors' views is compensated immediately after successful grasping by removing such parts of sensory data during consequent placing. As only the dimensions of the wall structure were known a priori and not its position or orientation, the RGB-D camera alone is used for wall

detection. The wall detection and computation of the placing position on the wall takes up to 10 ms. The brick placing uses its own dedicated state machine to manage various placement stages and considers that, e.g., only a part of the wall segment can be visible and the placement is planned to be on the leftmost free position on the wall.

The visual detection for autonomous wall building with drones has to be robust, fast, and with minimal computation demands. Detection during the scanning of the arena (i.e. looking for both bricks and walls) takes up to 15 ms, detection of brick with known color takes up to 5 ms, and the computation of brick placement on the wall takes up to 10 ms. The wall detection pipeline first detects the ground in the RGB-D data by creating a histogram of measured distances to ground plane transformed from RGB-D data using measurements from the Inertial Measurement Unit (IMU). A number of highest distance values in the histogram are used as altitude measured by the RGB-D sensor. Thresholding of the distances to ground plane using the measured altitude is then used to create a binary image with possible wall detections. Finally, the wall segments are verified by examining contour lines of the possible detections to be parallel and in distance approximately equal to wall width. Visual recognition of the bricks is mainly based on white plate detection using color segmentation applied to Hue, Saturation, Value (HSV) image from the color camera. The contours of white segments are transformed to a plane parallel to the ground plane in altitude equal to brick height. Such transformed contours are then checked for the size of the white plates. Finally, additional color thresholding of the HSV image is used to identify different types of the bricks. All detection functions take only one thread on the onboard computer, and therefore allow enough computation power for the rest of the system, e.g., control algorithms.

Automatic control of the UAV motion is vital for the precise grasping and placing of bricks. We build upon our success from the first MBZIRC 2017 challenge for which we developed a hybrid Model Predictive Control (MPC) tracking controller [5]. An MPC feedforward tracker is coupled with the geometric tracking controller [6] to minimize a control error around the pre-planned differentially flat dynamics and to provide us with attitude tracking. The tracking controller is part of the provided open-source UAV system [7]. The UAV system allows the use

a visual servoing technique to estimate the states of the UAV directly using observations of an object, i.e., the brick. With the visual servoing, the control feedback loop is closed using only the camera-based data and the onboard IMU. The visual servoing removes the inaccurate GPS localization from the loop for the duration of the grasping manoeuvre, significantly increasing the accuracy of the grasping manoeuvre to an order of centimeters. We empirically verified that relying on a traditional GPS introduces a significant localization position drift. The potential GPS drift impacts the UAV control performance to the extent of making a precise grasping manoeuvre an unfavorable probabilistic event. Furthermore, we employed a real-time scheduling of controller gains and dynamic constraints to satisfy the varying conditions during the various stages of the mission. This was especially important during the transitions between the GPS and visual servoing stages of the flight where the UAV feedback loop exhibited different properties, mainly due to changing noise and delay characteristics of the UAV state estimate.

In this paper, we present the overall approach and system that won, by a significant margin, Challenge 2 of the MBZIRC 2020 in autonomously placing the most bricks on the wall. The vision techniques for brick and wall detection that allowed for precise vision-based grasping and placing have been detailed in this paper. Description of the UAV control used in a closed-loop with the visual detection of the bricks and the wall is given. The multi-UAV cooperative wall building approach is described as well, including the state machine of individual UAVs, creation of a topological map of the arena, and the deterministic distribution of the multi-robot task. The whole system is open-sourced² to allow the community to further build on our successful system. Finally, the results from the competition along the lessons learned are described.

The remainder of this work is organized as follows — the rest of this section begins with an overview of related literature works and then details the MBZIRC Challenge 2. Section 2 introduces the hardware platform used for the wall building task. The UAV control system is presented in Sec. 3.1. The overall approach used for the task is then described in Sec. 4. Sections 5, 6, and 7 describe, in this order, the three most crucial parts of the wall building system: the arena scanning, brick grasping, and brick placing. Results achieved during the competition are discussed in Sec. 8 and conclusions are drawn in Section 9.

1.1. Related work

UAVs can be deployed in various scenarios in the field of construction [1]. Visual inspection of construction sites, area surveying prior to construction, and security and safety monitoring are examples of such tasks [3]. Inspection of existing structures, such as bridges [8], can also be considered among these scenarios. Nowadays, each of these tasks can be performed by considerably small UAVs that are manually piloted or semi-autonomous. However, UAVs participating directly in

physical construction and operating autonomously are still being considered, mainly in lab-controlled environments.

Authors of [9] proposed a system for building cubic truss-like structures from simple nodes by a team of UAVs. The system relies on a motion tracking system. Additional work on the assembly of truss structures has been explored by the authors in [10]. The main focus is on a distributed construction algorithm to build a truss according to a given blueprint using a team of UAVs. An approach for building tensile structures, such as structures from ropes, using UAVs is presented in [11]. The paper focuses on creating trajectories for UAVs with respect to a built structure and on the UAV control required for building elements with tension forces. Building bridges with cooperating UAVs using the tensile ropes is further described in [12]. Trajectory planning for UAVs for assembly and structure construction is proposed in [13]. The authors focus on collision-free planning for multiple UAVs performing the construction task. In [14], a group of four UAVs are used to build a tower from foam bricks. The paper describes the indoor application where the positions of bricks for grasping are predefined and UAVs rely solely on a motion capture system. The system is thus very informed about its environment and serves as proof of the concept of building structure from bricks by UAVs.

Research of UAVs for assembly and construction with a main focus being on multi-robot cooperative aspects was part of the ARCAS project [15]. An important capability of the UAVs for direct participation in construction is the aerial manipulation and physical interaction with structures being built. We refer to a thorough survey on the aerial manipulation [16]. In [17], control of aerial robots interacting with other objects is examined for cases such as UAVs equipped with an arm manipulator which could perhaps be used for building more complex structures. In [18], an autonomous aerial helicopter is also equipped with an industrial manipulator. A controller with kinematic coupling is proposed to improve operation with the manipulator onboard the UAV. Fully-actuated UAVs [19] can also be considered for construction tasks due to having higher stability during physical interaction from various tilt angles. Authors of [20] propose a planning approach for structure construction with multiple UAVs equipped with a robotic arm. The approach is addressed by consecutive assembly planning, task allocation planning, and action planning. In contrast with the approach proposed in this paper, none of the state-of-the-art publications solve all the sub-problems required for fully-autonomous operation, i.e., visual brick detection and localization, autonomous detection of the pickup and placement locations, mission scheduling for multiple UAVs, control, state estimation, and motion planning.

The herein presented grasping approach uses the visual servoing technique that was previously mentioned for grasping in [21]. The approach in [21] simplified the task to a one dimensional problem with an external motion capture system controlling other dimensions. Such simplification is not possible for a real outdoor experiment. The detection of an object for manipulation with a robotic arm is discussed in [22]. In this work, a stereo camera system is used for object detection in an outdoor environment without a motion capture system. The speed of

²https://github.com/ctu-mrs/mbzirc_2020_wall_building

object detection is slow, taking up to 1 s and unusable for UAV control and visual servoing. The presented work does not deal with object placing and presents only preliminary results.

In [23], an autonomous aerial pickup and delivery is approached by using a magnetic gripper. The paper focuses on a grasping device employing Electro Permanent Magnet (EPM) and on visual servoing for precise object grasping. The work is motivated by MBZIRC 2017. Similarly, the work [24] focuses on object pickup and delivery. However, both the pickup location and the delivery location are known and marked. Therefore, this task is similar to the gathering of ferrous objects in the MBZIRC 2017. The approach presented in this paper covers full visual servoing in all three dimensions. Furthermore, we do not rely on Global Navigation Satellite System (GNSS) Real-time Kinematics (RTK) thanks to our robust picking mechanism that can compensate for real-world phenomena.

Related to the previously discussed Challenge 2 of the MBZIRC 2020 is Challenge 3 (Ch3) of the MBZIRC 2017 which featured a treasure hunt scenario where metallic disk-shaped objects were searched for in an arena by three UAVs and collected to a common box. In contrast to the treasure hunt scenario, the wall building task requires additional precise placement on a wall and also features a UGV within the challenge. However, grasping with a magnetic gripper [25] and required cooperation of the UAV team are the same for both challenges. The team lead by Czech Technical University (CTU) won the treasure hunt scenario of the MBZIRC 2017 [26]. The approach [26] also contains initial scanning of the arena. However, the grasping in [26] does not use the herein employed visual servoing and instead uses a more precise RTK GPS. Most importantly, the collection box in the Ch3 of the MBZIRC 2017 was in an a priori known location and of decent size.

The proposed system for the MBZIRC 2017 Ch3 by University of Seville [27] uses a search phase where the arena is divided and cooperatively scanned. A centralized Ground Control Station (GCS) is used for object detection stochastic filtering and further heuristic cooperative planning is used to assign individual UAVs to collect particular detected objects. The GCS also resolves potential conflicts and minimizes probability of collision. The object detection uses color segmentation and clustering, while the grasping employs a visual-based controller to precisely hit the target. The drop is done using the priori known position of the dropping box. The employed UAV platform uses standard GPS and IMU localization while the pickup mechanism uses EPM [28].

Team from ETH Zurich [29] for Ch3 of the MBZIRC 2017 used an approach with repeated switching between exploration and greedy pickup of the closest detected object with consequent delivery. The exploration uses a predefined zig-zag path during the scanning of an assigned arena part and switches to pickup/delivery mode once a valid target is detected. The system is decentralized with minimal data sharing of odometry for collision avoidance and drop box semaphore for dropping synchronization. The object detection is based on color thresholding and a blob detector with consequent classification of blob geometrical shape features for filtering. The detected objects are further tracked and used for pose-based visual servoing. The

Nonlinear Model Predictive Controller (NMPC) [30] is used for trajectory control. The localization is based on a combination of RTK GPS and visual-inertial odometry. The grasping employs EPM [28] gripper with Hall effect sensors grasp feedback.

Approach of the University of Bonn [31] for the Ch3 of the MBZIRC 2017 divided the arena into sectors with one for each drone. Each UAV broadcasts its position, navigation target, flight state, and detected objects outside of its own sector. Exploration of each sector is done with one UAV using a spiral pattern with random start. Object detection defines the likelihood of pixels belonging to colored object to be used further in the blob detector. The detected blobs are filtered based on blob shape and color parameters. The approach uses visual detection of the drop box in contrast to other teams. A variant of MPC based on precise trajectory generation [32] is used for controlling the UAVs. The UAV platform uses standard GPS and IMU, and the grasping device uses an electromagnet on a telescopic rod with a ball joint.

The above presented systems addressing the MBZIRC 2017 challenge [29, 31, 27] including the winning solution [26] do not provide sufficient mechanisms for solving the 2020 challenge, despite being state-of-the-art in the field. The aforementioned solutions require delivery of much larger objects that pose more difficult requirements on the precision of grasping and control. The placement of the objects is a key factor, which did not need to be solved in the previous installment of the challenge. The 2020 challenge requires precise placement of the bricks in 3D environment, which is even more challenging due to implied higher risk for the UAV since the UAV is required to fly nearby a complex 3D structure.

Overall, the presented wall building task of MBZIRC 2020 featured a very challenging scenario that required both autonomous outdoor grasping and placing using onboard sensors only. So far, such construction tasks were restricted mostly to controlled lab environments with motion capture systems or were not entirely autonomous. Furthermore, Challenge 2 of the MBZIRC 2020 is more complex than the former Ch3 of the MBZIRC 2017. The wall in MBZIRC 2020 has to be localized automatically due to its arbitrary position in each round and the brick placement has to be very precise for a brick to stay on the wall after placement.

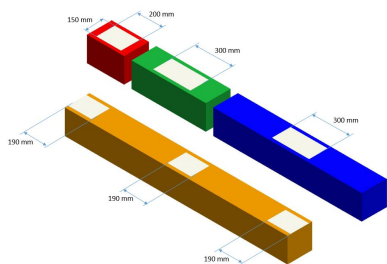
1.2. Problem overview

Challenge 2 of the MBZIRC 2020 featured a wall building task carried out by three UAVs and one UGV. Different wall placement areas and stacks of bricks with which to build were assigned for the UGV and for the UAVs. The layout of the wall building arena, with size of $40 \times 50 \times 20$ m, can be seen in Fig. 7. This paper concerns the UAV part of the Challenge 2, therefore we will further focus on the challenge details concerning this part. A total of four colored brick types — RED, GREEN, BLUE, and ORANGE — were available for possible placement on a wall, each with different weight, shape, and points for placing. Table 2 summarizes length, weight, and scoring of each brick type.

The ORANGE brick could be carried and place by a single UAV or by a group of UAVs. However, the UAV size was

Brick color	Length/m	Weight/kg	Score
RED	0.3	1.0	6
GREEN	0.6	1.0	8
BLUE	1.2	1.5	10
ORANGE	1.8	2.0	20

(a) Brick sizes, weights, and score points.



(b) Illustration of the bricks' visuals.

Figure 2: Parameters of the bricks present in Challenge 2 of the MBZIRC competition [4].

penalized if it exceeded a dimension limit, so a collaborative approach was encouraged. Each brick was also equipped with a ferromagnetic white plate in the middle (and additionally to the sides of the orange brick) to be grasped by a magnetic gripper allowing for multi-robot grasping. Initial layout of the brick stack for the UAVs was in 8×4 m area with six rows of bricks where two were reserved for 24 RED bricks, two for 12 GREEN bricks, one for six BLUE bricks, and one for four ORANGE bricks. The UGV had a different brick stack area that was distinguishable from the UAV stack by its properties, as later discussed in Sec. 5.

The wall for UAVs had a shape of the letter ‘W’ and consisted of four segments. Each segment was 4 m long and placed on a 1.7 m high base. Convex U-shaped channels with transparent sides were attached to the top of the segments to simplify placement and to support the already placed bricks in case of wind. The order in which the bricks were supposed to be placed on the wall was given just before the trials in order to build a wall in a given pattern. The given wall pattern consisted of randomly ordered 4 RED, 2 GREEN and 1 BLUE brick for each layer of the first three segments. The last channel was reserved for ORANGE bricks and can fit two such bricks per layer. Each UAV channel could contain two layers. The final score was based on reward of placed bricks and was further decreased based on number of mistakes in the given wall pattern using a rather complicated formula not relevant to the approach description. Therefore, the goal of Challenge 2 was to build as many bricks as possible according to the wall pattern within 25 minutes of the challenge trial.

2. Hardware platform

This section describes the UAV platform shown in Fig. 3 which was used for all UAVs deployed by the CTU-UPenn-NYU team in Challenge 2 of the MBZIRC 2020.

The utilized UAV quadrotor platform is composed of only commercial off-the-shelf (COTS) parts and rather inexpensive components and sensors. The brick and wall detection relies on one fish-eye color camera and one RGB-D camera. The global localization of the UAVs in the arena is based on a standard GPS receiver accompanied by Light Detection and Ranging (LiDAR) sensor for measuring altitude. The grasping was done using an in-house designed electromagnetic gripper with grasp feedback sensors. Finally, the basic stability of the platform was controlled by COTS flight controller governed by an onboard miniature computer that was used for all computations and autonomy during the wall building task.

The platform is based on the *Tarot 650 Sport* quadrotor frame with four *Tarot 4114 320Kv* motors, each connected to *BLheli32 51A* electronic speed controller and equipped with a 15-inch carbon fiber propeller. The thrust of individual motors, and thus the lowest-level control of the platform, is governed by the *PixHawk 4* flight controller which receives angular rate and total thrust commands from the control pipeline running on the onboard computer. The primary localization system is based on the *ublox Neo-M8N* GPS receiver connected to the flight controller. *Intel NUC Kit NUC8i7BEH* with *Intel i7-8559U* processor and 8 GB of RAM are used for onboard high-level computations including calculation of control commands, high-level planning, brick and wall detection, and others. *Ubuntu 18.04 LTS* operating system is installed along with Robot Operating System (ROS) [33] Melodic flavor which integrates the whole UAV software system.

Apart from the GPS-based localization, the *Garmin LiDAR Lite v3* distance sensor is used to measure the UAV altitude above ground. Brick detection, primarily during grasping, uses the RGB *mvBlueFOX-200w* camera with global shutter, 752×480 px resolution, and up to 93 frames per second (fps). The fish-eye camera lens *Sunex DSL215* is used to significantly enlarge the footprint of the camera on the ground. The camera is set to 20 fps, which is a sufficient value for visual servoing during grasping. To avoid obstruction of both the LiDAR and the mvBlueFOX camera by the grasped brick, both sensors are placed on the left side of the platform using a custom holder. Figure 3 shows the placement of the individual sensors on the platform. Down-facing *Intel RealSense D435* RGB-D camera, with depth Field-of-View (FOV) of $\approx 90^\circ \times 58^\circ$ and range of up to 10 m, is primarily used for the wall detection. Depth resolution of the RealSense is up to 1280×720 px with a frame rate up to 90 fps. For this challenge, the resolution 848×480 px is used with 30 fps. The RealSense camera is mounted under one of the motors and rotated towards the geometric center of the UAV. The mounting points of both RealSense and mvBlueFOX cameras enable navigation close above the walls and bricks.

Grasping of the bricks is done using two *YJ-40/20* electromagnets, each with up to a 25 kg equivalent of holding force. The magnets are connected to a common rod equipped with a

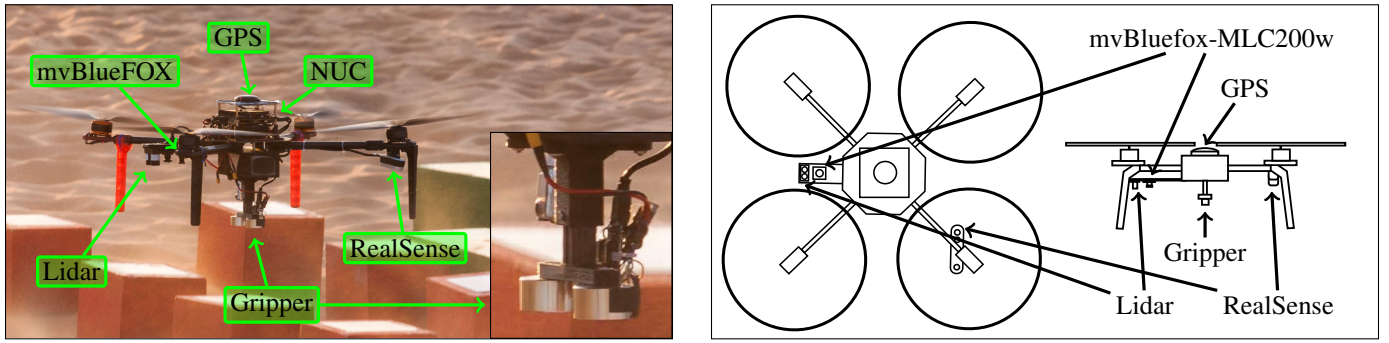


Figure 3: UAV platform for the brick challenge.

spring mechanism along the z-axis for dampening the shocks when landing on a brick gripper-first. Each magnet is equipped with an integrated Hall effect sensor to verify proper attachment of the ferromagnetic part of the brick to the magnet. The electromagnets are rated to operate at 12 V, however, operation at 24 V is selected instead to further increase the grasping force at the cost of higher power consumption and heating.

3. Preliminaries

3.1. UAV control system

Multirotor UAVs are notable for their inherently unstable dynamics. Continual corrections to their flight need to be supplied by a feedback controller at a rate of approximately 100 Hz to maintain stable flight. Moreover, automatic feedback control requires an accurate estimate of the UAV dynamical system states. The tasks of state estimation and feedback control are complemented by several others, such as automatic feedback reference generation, trajectory following, take-off, landing, and more. All these vital subsystems are encapsulated in the *MRS UAV System* [7], an open-source³ standalone and general control pipeline (see Fig. 4). The *MRS UAV System* was used by the CTU-UPenn-NYU team in all the challenges of the MBZIRC 2020 competition. The provided framework aids deployment of autonomous UAVs, allowing focus mainly on the diverse scenarios of the competition. It relies on the PixHawk embedded flight controller to control the UAV attitude rate ω and thrust T , while the rest of the pipeline is executed on an onboard high-level computer. The *Mission & navigation* block, which is the core topic of this manuscript, provides the *MRS UAV System* with desired trajectory references to fulfill the objectives of the challenge.

3.2. UAV state estimation

The state estimation part of the *MRS UAV System* fuses data from onboard sensors into multiple independent hypotheses of the UAV state. In context of this particular challenge, the UAV

state is estimated using three individual estimators: a GPS-based localization, an optic-flow odometry, and visual servoing relative to an observed brick. These three sources of localization can be used independently depending on the particular situation. Transitions between the stack of bricks and the wall area is made using the GPS-based estimation and the grasping of a brick is achieved via the visual servoing. The optic-flow estimator is used as a backup in case the visual servoing fails. The *MRS UAV System* provides a state estimate consisting of the UAV *body frame* (\mathcal{B}) position $\mathbf{r}^{\mathcal{B},\mathcal{W}}$ and orientation $\mathbf{R}^{\mathcal{B},\mathcal{W}}$ within a *world frame* (\mathcal{W}). Figure 5 depicts the coordinate frames used within the control pipeline. The absolute position of the *world frame* depends on the actively used state estimator. When the state estimator is changed, the control pipeline synchronizes a virtual jump between the old and new coordinate frame, such that it is not noticeable to an outside observer.

3.3. UAV feedback control and tracking

The *tracking controller*, as depicted in Fig. 4, encapsulates a MPC feed-forward tracking approach [5] for generating a smooth control reference and a *geometric tracking controller on $SE(3)$* for tracking the control reference [6]. We also utilize an alternative MPC-based feedback controller [7], when the state estimate provided by the onboard estimator might be unreliable (e.g., while grasping a brick). The input to the control pipeline, supplied from the *Mission & navigation* block, can be a 3D position and heading reference (\mathbf{r}_d, η_d) or a time-parametrized reference trajectory

$$\{(\mathbf{r}_d, \eta_d)_1, (\mathbf{r}_d, \eta_d)_2, \dots, (\mathbf{r}_d, \eta_d)_k\}. \quad (1)$$

4. Autonomous multi-UAV wall building

This section describes the proposed high level approach for the wall building task, the state machine of individual UAVs, and the approaches used for the multi-robot coordination of the task. The proposed approach for wall building is designed to distribute the task among the three UAVs as much as possible while mitigating possible mutual collisions. Furthermore, we refer to the individual UAVs as UAV1, UAV2, and UAV3. The task starts with UAV1 scanning the arena in order to find the positions of the wall and the stack of bricks for the UAVs.

³http://github.com/ctu-mrs/mrs_uav_system

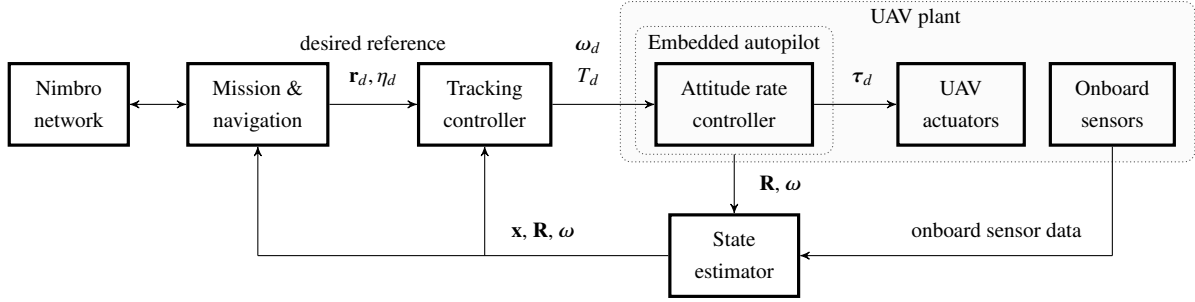


Figure 4: A diagram of the system architecture. The *Mission & navigation* part supplies position and heading reference (\mathbf{r}_d, η_d) to a tracking controller. The *Tracking controller* encapsulates feed-forward tracking and feedback control techniques to produce desired thrust and angular velocities (T_d, ω_d) for the Pixhawk embedded flight controller. The *State estimator* fuses data from onboard sensors to create an estimate of the UAV translation and rotation (\mathbf{x}, \mathbf{R}). The *Nimbro network* manages communication between the UAVs and allows execution of a coordinated multi-robot scenario.

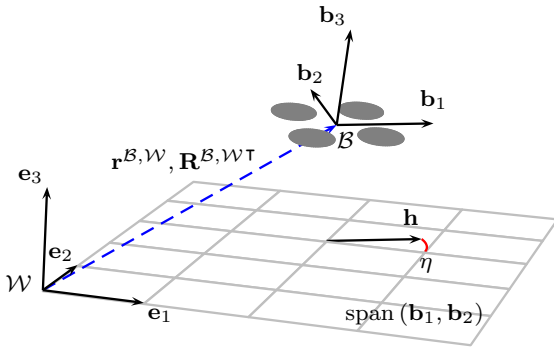


Figure 5: The image depicts the world frame $\mathcal{W} = \{\hat{\mathbf{e}}_1, \hat{\mathbf{e}}_2, \hat{\mathbf{e}}_3\}$ in which the 3D position and orientation of the UAV body is expressed. The body frame $\mathcal{B} = \{\hat{\mathbf{b}}_1, \hat{\mathbf{b}}_2, \hat{\mathbf{b}}_3\}$ relates to \mathcal{W} by translation $\mathbf{r}^{\mathcal{B},\mathcal{W}} = [x, y, z]^T$ and rotation $\mathbf{R}^{\mathcal{B},\mathcal{W}^T}$, respectively. The UAV heading vector \mathbf{h} , which is a projection of $\hat{\mathbf{b}}_1$ to the plane $\text{span}(\hat{\mathbf{e}}_1, \hat{\mathbf{e}}_2)$, forms the heading angle $\eta = \text{atan2}(\hat{\mathbf{b}}_1^T \hat{\mathbf{e}}_2, \hat{\mathbf{b}}_1^T \hat{\mathbf{e}}_1) = \text{atan2}(\mathbf{h}_{(2)}, \mathbf{h}_{(1)})$.

The scanning process is described in detail Sec. 5. After scanning, the positions of mapped wall channels and the individual brick type stacks are shared to the other UAVs (UAV2 and UAV3). Each UAV is then assigned to one of the three first (non-ORANGE) channels to build the bricks sequentially from one side according to the given pattern for individual channels. The brick stack area is also divided along the longer side, such that UAV1 and UAV3 are grasping from the sides and gradually progressing to the middle of the area with each grasped brick, while UAV2 is grasping from the middle part of the area. However, due to the UAV stack area being a size of 8×4 m, only UAV1 and UAV3 were flown simultaneously in the competition while UAV2 waited till the others have finished their mission to increase safeness. The task then proceeds with grasping and placing according to the wall pattern assigned to each individual UAVs. The sensor connection and battery state are checked before each grasping begins and the UAV lands after task completion or in the case of battery depletion. The used state machine is further described in the next section while the multi-robot aspects are detailed in Sec. 4.2.

4.1. UAV state machine

The state machine used onboard each UAV to solve the wall building task is depicted in Fig. 6. It is implemented in FlexBE Behavior Engine [34] based on the state machine framework SMACH [35]. The whole system is integrated in the ROS.

The state machine starts by the *Prepare UAV and wait for start* procedure [S1] that initializes all UAV system parts, arms the UAVs, and awaits trigger from remote control to start wall building task. The scanning UAV1 then preforms *Take-off* [S2] immediately after the task starts. Meanwhile, both UAV2 and the UAV3 are in the *Wait for map* state [S3] where they wait for arena map shared from UAV1. UAV1 scans the arena (*Scanning procedure* [S5]) detailed in Sec. 5 then shares the four mapped wall channels and brick stack designed for the UAVs. When the map is received by UAV3, it continues with *Take-off* [S2] as it is used with UAV1 for simultaneous wall building. UAV2 waits for the other two drones to land (*Wait for finish* state [S4]) before continuing with the *Take-off* and further building of the wall. The wall building then continues with *Assign wall and bricks plan* state [S6] that contains the deterministic method that assigns different wall channels, flight altitude, and grasping positions above the brick stack to each UAV. This state creates a plan of individual grasping and placement attempts according to assigned channel pattern. It is discussed more in the following Multi-robot coordination section. The UAVs then proceed with *Assign next brick* state [S7] that selects the next brick according to the plan (assuming there are still bricks in the plan to be placed). If not, the UAV switches to *Land* procedure [S8] and lands at the UAV take off position. Before attempting the actual grasping, the *Check UAV* state [S9] makes sure that the sensors necessary for the grasping and placing tasks are connected. Furthermore, the battery state is checked and if both the sensors and the battery are in ready-to-fly conditions, the UAV proceeds with grasping. Otherwise, the UAV switches to the *Land* procedure. In the *Grasping* procedure [S10], the UAV initially flies to the mapped grasping position for the current brick type in the stack that is assigned to the particular UAV. Afterwards, the procedure continues to the lower-level grasping state machine that includes, e.g., visual brick servoing for precise relative positioning of the UAV above the brick, as is

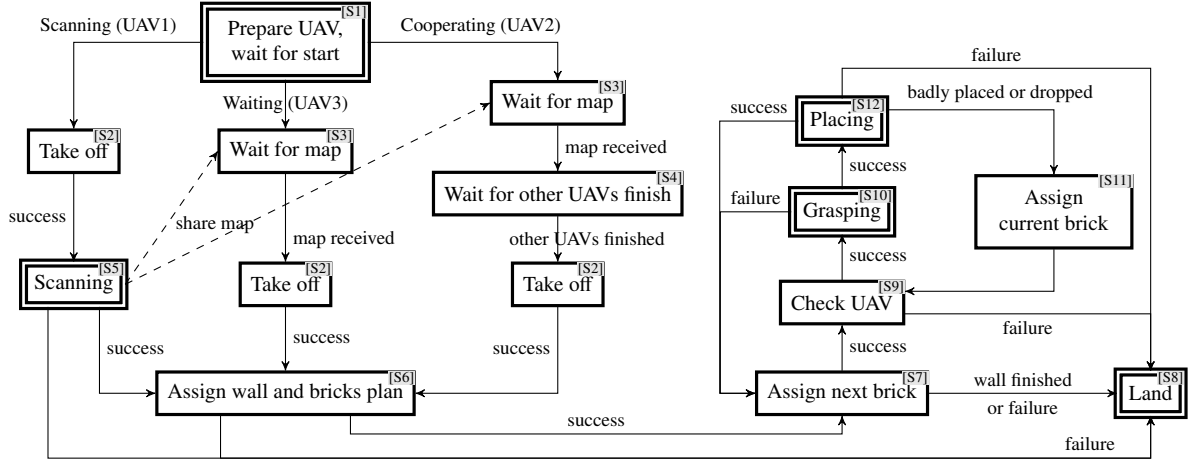


Figure 6: UAV state machine for the wall building task.

described in Sec. 6. In case of grasping failure, the UAV continues with assigning the next brick from the plan in order to try, e.g., a different brick type or brick closer to the middle stack area in case of side UAVs. When the grasping is successful, the *Placing* procedure [S12] starts with flying (with a heading minimizing the brick air resistance) to a designated wait position next to wall using the assigned flight altitude. It then flies to the fixed altitude above the mapped position of the assigned wall channel where a lower-level placing state machine begins. During the placing procedure, the brick is checked for having been dropped or being badly placed. In both cases, the same brick is assigned in *Assign current brick* state [S11] and the UAV proceed with check and grasping. In case of successful placement, the wall building continues to the next brick in the plan [S7]. Notice that all states [S5], [S6], [S7], [S9], and [S12] can result in failure that would switch the UAV to landing at take-off position. However, almost all states contain an additional hard failure mode in which the UAV performs an emergency landing at its current place.

4.2. Multi-robot coordination

The multi-robot coordination with three UAVs for the wall building task was proposed on two levels: the first being based on communication and the second utilizing known arena properties and thus mitigating possible UAV collisions.

The communication between UAVs is based on 5 GHz Wi-Fi network together with the *NimbroNetwork* [36] ROS package that handles sharing certain messages over Wi-Fi. The continuously shared messages are the predicted trajectories and diagnostics of the used onboard MPC [5]. The predicted trajectories are mainly used for collision avoidance purposes while the diagnostics is used as a “heartbeat” of the flying UAVs to be used, e.g., for triggering UAV2 take-off after other UAVs finish or stop responding. Furthermore, the current drone positions and the arena map are shared among the UAV team. The arena map is shared from the scanning UAV1 once the scanning is finished and is used to proceed from the *Wait for map state* [S3]. The map itself contains position and rotation $(x, y, heading)$ of

all four wall channels and line segments along the individual brick types.

The arena properties that are used to mitigate collisions are the possible partitioning of the UAV wall into four channels and the division of the brick stack area to three parts along the longer side. Only the first three wall channels (non-ORANGE) are handled, each by different UAV and filled sequentially from one side according to the given wall pattern (i.e., from the left in the case of Fig. 7). Each UAV has its own brick stack part where the grasping maneuver of selected brick type starts at the mapped line of that particular brick type (see Fig. 7a). UAV1 and UAV3 begin grasping initially on the outside of their brick stack parts and gradually progress to the middle. UAV2 starts the grasping maneuver in the middle of its part. Furthermore, the stack part of UAV1 and UAV3 are optionally swapped, minimizing the distance between a particular channel and stack part. Finally, each UAV has its own flight altitude ($z \in \{3.0, 4.0, 5.0\}$ m) that is used between the assigned stack part and wall channel. See Fig. 7a for the arena layout and partitioning of the individual wall channels and brick stack among the UAVs.

5. Scanning for bricks and wall placement

The proposed approach begins with scanning the arena as the brick stack and wall channel locations are initially unknown. The scanning task as described throughout this section includes planning of the scanning path, detection of both the bricks and wall channels, filtering and tracking of the detections, and, finally, in creation of the topological map of the brick stack and wall channels.

5.1. Path planning for scanning the arena

The path planning for scanning of the arena is a task of coverage path planning [37] where the entire arena has to be covered with both the RGB BlueFOX camera and the RGB-D RealSense sensors. The whole task is handled by one UAV as topological map creation from multiple UAVs would require

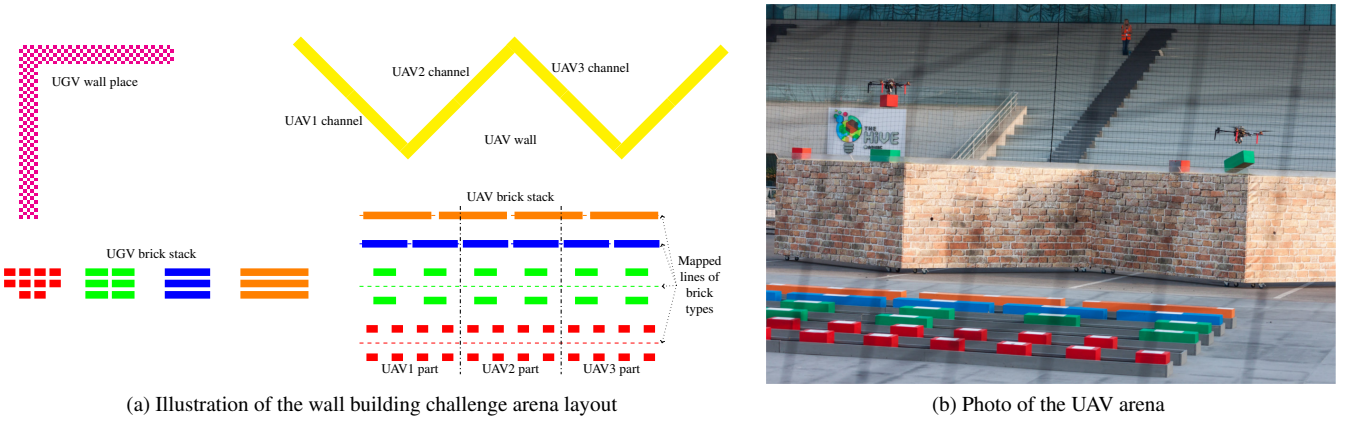


Figure 7: Wall building challenge arena layout (a) and photo from the competition (b).

a high-bandwidth network and synchronization of all detections. The path is composed of classical zig-zag primitives with smooth curvature constrained by turning radius ρ computed as $\rho = v_t^2/a_{max}$. The used turning velocity v_t and maximal acceleration a_{max} are 1.5 m s^{-1} and 2 m s^{-2} , respectively. Scanning speed is however 3 m s^{-1} , meaning that the scanning UAV is accelerating and decelerating after and before turns. The final zig-zag path, as shown in Fig. 21 in the Sec. 8, is then calculated with respect to the $\approx 90^\circ$ RealSense horizontal FOV (which is smaller than the BlueFOX camera lens), and also with respect to the set scanning altitude of 4.5 m (due to limitations of the RealSense distance measurements quality).

5.2. Wall detection

The wall detection method uses the onboard RealSense D435 sensor. As mentioned in [38], the accuracy of this sensor depends on the selected resolution and parameters of the sensor. The RealSense was dedicated for the improvement of brick detection primarily from short distances. Therefore, the image resolution was set to $848 \times 480 \text{ px}$ with a minimal detection distance of 0.175 m. The selected resolution has a further influence on depth accuracy. Therefore, while scanning from altitude 4.5 m, the root mean square (RMS) error of the distance measurements is $\approx 0.6 \text{ m}$. Such measurement error is for the worst case scenario in an outdoor environment where it also depends highly on the target's texture.

The first step of the wall detection method is to find the ground plane. As the UAV orientation is known, it only seeks to find the UAV height above the ground. The arena for Challenge 2 had an almost flat surface with the brick height at 0.2 m, the pillar of bricks for UGV with 0.6–0.8 m height, and a wall height of 1.7 m. The UAV is equipped with down-pointing Garmin LiDAR lite v3 sensor to measure UAV height, but the sensor can also point to an obstacle. The LiDAR height measurement was not used during the grasping or placing of a brick. Instead, we used a ground plane distance estimated from the RealSense stereo camera. The orientation of the UAV is estimated using the onboard IMU (tilt) and magnetometer (heading).

To speed up the detection, the input depth data with resolution $848 \times 480 \text{ px}$ are reduced to resolution $106 \times 60 \text{ px}$ by selecting minimal valid value (greater than zero) from each $8 \times 8 \text{ px}$ sub-image. The minimal value filter is used to reduce the size of the input data and to simultaneously remove outliers with invalid data of zero or measurements that are higher than actually possible.

The measured sensor data are then rotated to the world coordinate system. The depth measurement $d = d(x, y)$ represents a 3D point

$$\mathbf{p} = \left[d \cdot \frac{x - c_x}{f_x}, d \cdot \frac{y - c_y}{f_y}, d \right]^T, \quad (2)$$

where c_x, c_y, f_x, f_y are parameters of the RealSense camera received from factory calibration. Firstly, we transform the measurements \mathbf{p}^S from the sensor frame S to the UAV body frame B as

$$\mathbf{p}^B = \mathbf{R}^{S,B} \mathbf{p}^S + \mathbf{r}^{S,B}, \quad (3)$$

where $\mathbf{R}^{S,B}$ is the rotation from S to B and $\mathbf{r}^{S,B}$ is the translation from S to B . We then similarly transform the measurement from the body frame B to the world frame W :

$$\mathbf{p}^W = \mathbf{R}^{B,W} \mathbf{p}^B + \mathbf{r}^{B,W}. \quad (4)$$

Therefore, the final transformation is written as

$$\begin{aligned} \mathbf{p}^W &= \mathbf{R}^{B,W} (\mathbf{R}^{S,B} \mathbf{p}^S + \mathbf{r}^{S,B}) + \mathbf{r}^{B,W} \\ &= \mathbf{R}^{B,W} \mathbf{R}^{S,B} \mathbf{p}^S + \mathbf{R}^{B,W} \mathbf{r}^{S,B} + \mathbf{r}^{B,W}, \end{aligned}$$

to obtain $\mathbf{p}^W = [p_x^W, p_y^W, p_z^W]^T$. However, for object detection only the z component p_z^W is important and $\mathbf{R}^{B,W} \mathbf{r}^{S,B} + \mathbf{r}^{B,W}$ is constant for one measurement. The altitude of the point representing depth measurement $d = d(x, y)$ at pixel coordinates $[x, y]$ is defined as

$$p_z^W = d \cdot \mathbf{R}_z \left[\frac{x - c_x}{f_x}, \frac{y - c_y}{f_y}, 1 \right]^T + \mathbf{r}, \quad (5)$$

where $\mathbf{R}_z \in \mathbb{R}^3$ is the last row of the rotation matrix $\mathbf{R} = \mathbf{R}^{\mathcal{B}, \mathcal{W}} \mathbf{R}^{S, \mathcal{B}}$ and \mathbf{r} is a constant value for one measurement. This simplification speeds up computation by 3 times.

The altitude of the UAV is then computed from a histogram of altitudes of all points in the reduced 106×60 px image. Based on the experimental evaluations in desert environment prior to the competition, altitude of the UAV is estimated as a value for which more than 1000 px have a larger or equal measurement. If the detected distance is bigger than 3.5 m, the accuracy of the RealSense sensor decreases and the UAV altitude combines the Garmin LiDAR measurement and RealSense measurement.

The next step is to create a binary image I_{thr} by thresholding all pixels with an altitude higher than 1 m above the ground (the height of the wall is 1.7 m and the accuracy of the RealSense sensor from an altitude of 5 m is 0.6 m). The following steps in the Alg. 1 use the OpenCV functions [39].

Algorithm 1: Wall detection

Input: I_{thr} – thresholded image
Output: (x, y, α) — center of the wall segment with α wall rotation

```

 $I_{clo} = morphology\_close(I_{thr})$  // OpenCV functions
erode, dilate
 $Contours = findContours(I_{clo})$  // OpenCV functions
findContours
 $Contours_{transform} = \emptyset$ 
for  $p \in Contours$  do
    if  $p$  is not at border then
        Add  $R \cdot p$  into list  $Contours_{transform}$ 

 $Lines_{approx} = approxPolyDP(Contours_{transform})$  // OpenCV
functions approxPolyDP
for  $l_1, l_2 \in Lines_{approx}$  do
    if  $|l_1 \times l_2| < thr_1$  then //  $l_1$  is parralel to  $l_2$ 
        if  $|l_1 - l_2| \approx wall\_width$  then // distance  $l_1$  to
         $l_2$  is correct
            output  $(x, y, \alpha)$  —  $(x, y)$  is center between  $l_1$  and
             $l_2$ ,  $\alpha$  — is  $l_1, l_2$  orientation

```

The functions *morphology_close*, *findContours*, and *approxPolyDP* are from OpenCV library. The last step of the Alg. 1 is testing for whether the distance between two lines is correct. This test compares the distance of endpoints of one line from the second line and vice versa, but this test does not recognize whether the lines are parallel and opposite to each other. To test this feature, the minimal rectangle that contains all endpoints of both lines is created. The length of this rectangle has to be less than a 0.8 sum of both lines and the width of this rectangle should be approximately equal to wall width, 0.25–0.40 m. Positions of the lines with respect to minimal rectangle is shown in Fig. 8.

The results and various stages of the wall detection method are depicted in Fig. 9.

5.3. Brick detection

Detection of the bricks using the mvBlueFOX color camera is based on the white plate detection in the center of each brick.

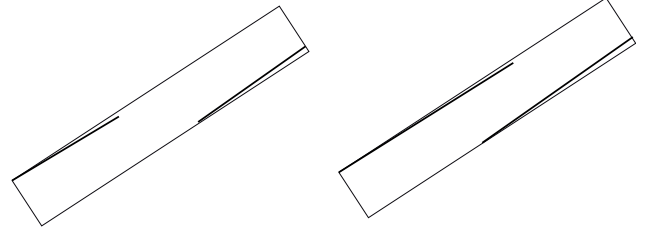


Figure 8: Positions of the wall border lines in a minimal containing rectangle. Wrong position of the parallel lines is show on the left and the correct position on the right.

Table 1: HSV ranges for color segmentation.

	Hue		Saturation		Value	
	min	max	min	max	min	max
<i>White</i>	0	180	0	60	180	255
<i>Red1</i>	0	8	70	255	80	255
<i>Red2</i>	160	180	70	255	80	255
<i>Green</i>	44	80	60	255	60	255
<i>Blue</i>	80	130	60	255	60	255

The position of a brick in global world is based on known altitude and orientation of UAV and the known brick height. The white detection is based on simple color segmentation using OpenCV function *inRange()* applied to a HSV image. The HSV image is created by function *cvtColor* (for color space conversion) from the original color camera data. The HSV image is further used for red, green, and blue detection. The parameters for white, red, green, and blue segmentation are listed in Table 1, where hue is from interval $\langle 0, 180 \rangle$, with saturation and value from interval $\langle 0, 255 \rangle$.

The method that finds a white plate in the segmented image is described in Alg. 2. After segmentation, the image is processed by morphological *closing* operation and the contours are computed by OpenCV *findContours()* function with chain simple approximation. All points on contours are then undistorted and transformed into a plane parallel to the ground plane with height equal to the brick height of 0.2 m. The lenses used for the color camera are very wide with a horizontal FOV of 185° ; therefore we use the *Ocam toolbox* [40] for omnidirectional cameras. The undistortion operation is done simultaneously with the rotational transformation to the global coordinate system in order to speed up the computation. Finally, a convex hull of points in the global coordinate system is found and used for brick classification.

If the entire white segment is inside the camera image, then the correctness of detection depends only on the size of the minimal rectangle area that contains the border of white segment transformed into the world coordinate frame. If the UAV is close to the brick, the white segment can cross the border of the image, so that the entire white plate is not in the camera image. If the white segment forms a U shape (i.e. shape from two parallel lines and one perpendicular line) then the center of the brick can be calculated not as the center of the transformed

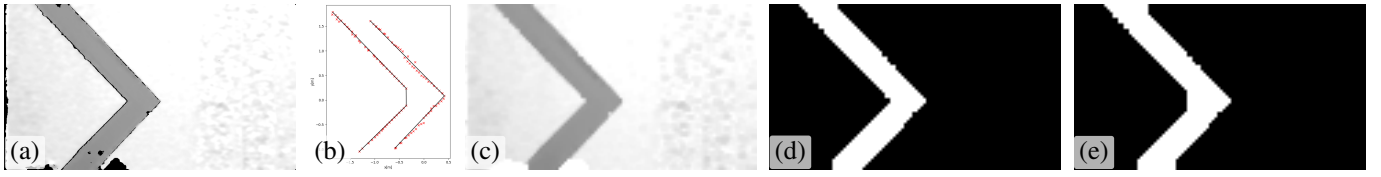


Figure 9: Original depth data (a) used for computing the result of the wall detection (b). The depth data are first filtered to lower resolution (c), then thresholded using wall height (d), and applied with the morphological *closing* operation (e).

area, but as a point with correct distance from the transformed border.

The results of the brick detection algorithm from the scanning altitude 4.5 m are depicted in Fig. 10. Details of transformed points to a global coordinate system with illustrated brick detection is shown in Fig. 11. The better and more accurate detection from a lower altitude is depicted in Fig. 12. In results from brick grasping (see Fig. 13), it can be noticed that only part of the white plate is visible and the correct brick position has to be calculated from the border shape.

5.4. Brick and wall filtering

Each detected brick and wall segment is filtered and placed in a map. The map consists of a bank of Linear Kalman Filters (LKFs) that maintains a smooth hypotheses of each object and provides stable references during grasping and placing attempts. Upon detection, each object is first checked for a series of preconditions to be later fused in the map:

- the object is excluded, if its coordinates are within 5 m from other UAV target,
- objects situated outside of the designated challenge area are excluded,
- bricks whose attempt to grasp was previously unsuccessful is excluded,
- wall segments outside the expected height range [1.0, 2.3] m are excluded.

The objects which pass the preconditions are matched with their nearest neighbour in the map. In the case of a brick, a standard correction to the LKF is formed, containing the brick's x , y , z world coordinates and heading. The wall segments also contain their length, which is an important factor for matching the measurements to the map. The wall segment detections are projected orthogonally to a candidate hypothesis to obtain a measure for evaluating the similarity of the segments. When no match is found for the detected object, a new instance of LKFs is created and placed in the map. Each hypothesis in the map maintains a counter for the number of corrections that were applied to the instance of the LKF.

Post-processing of the map is applied periodically during flight to merge nearby hypotheses by combining their states in the ratio of the number of corrections in each hypothesis. This is required due to the drift of the GPS localization system which causes the objects to drift even in the time span of a single flight.

The post-processed detection map is later used to obtain a topological estimate of important sectors in the map (e.g. UAV wall area, UGV wall area, UAV brick area, and UGV brick area).

5.5. Topological map creation

The wall and brick detections are saved and filtered in the detection map during the entire scanning flight in order to create the topological map of the arena. It is essential to precisely map positions of the wall channels and the individual brick type stacks (as shown in Fig. 7a), to determine wall building plans for individual UAVs. Map creation had to manage possible wrong detections, filter out the UGV bricks present in the arena, and correctly decide the order of wall channels to follow for the prescribed wall pattern. Figure 22 in the results section shows an example of the mapped wall channels and bricks.

The brick and wall detections received from the detection map are handled separately as they were placed independently in the arena. Initially, all bricks with a low number of corrections (empirically set to 6 corrections) are filtered out and considered detection noise. Next, a Gaussian Mixture Model (GMM) [41] for two clusters is estimated using the detections' (x, y) position in order to separate UAV and UGV brick stacks. Only the detections which are close (within 6 m) to one of the two cluster means are kept and a Principal Component Analysis (PCA) [42] with two components (due to the data being two-dimensional in (x, y)) is applied to both clusters. The PCA returns two variances for each cluster effectively proportional to width and height of the arbitrarily rotated UAV and UGV brick stacks. The UAV stack is then selected as the one with the larger width. A median filter together with outlier removal (bricks farther than 8 m from the median) is then iteratively used for the UAV stack until the median converges, or for a limited number of iterations. The line segments along the brick types (see Fig. 7a and Fig. 22b) are formed from the brick (x, y) mean position of individual brick types and from the median heading of all remaining bricks.

The walls from the detection map are also first filtered out in case of no corrections of the particular wall. The iterative median filter with outlier removal (of wall centers farther than 10 m from the median), similar to the one for the brick detections, is then used to find the most perspective location of the 'W' letter-shaped wall segments (see Fig. 7a). After the median filtering, the remaining wall segments are clustered together such that each detection is assigned to a cluster with horizontal distance within 3 m and heading distance within 0.5 rad. The average position and rotation of the clusters are then assumed to

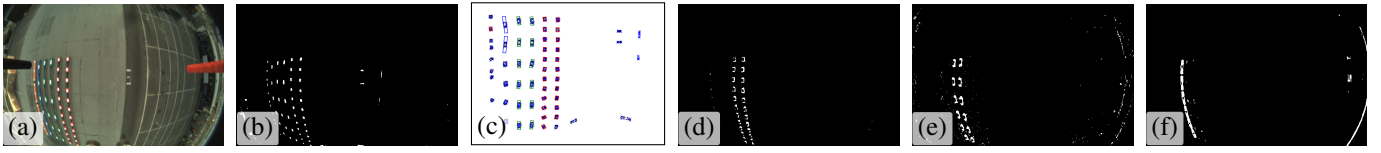


Figure 10: Brick detection based on an original color camera image (a) with consequent white color segmentation (b) and contour detection (c). The segmentation results are shown for red (d), green (e), and blue (f) colors.

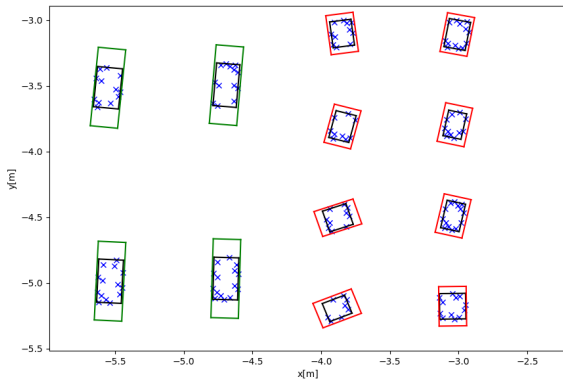


Figure 11: Detail of contours and brick detection results from Fig. 10 including the incorrect orientation of several bricks from scanning altitude.

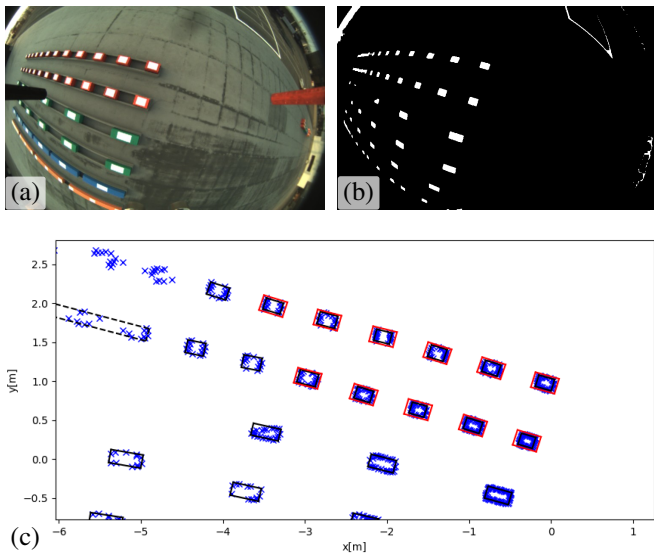


Figure 12: An original image from the color camera, white color segmentation result, and the contours and brick detection results.

be the individual wall channels. Line intersections of such wall channels are used to decide the order of wall channels in the ‘W’ letter shape while only intersections within short distance (≤ 6 m) from channel centers and with rather perpendicular mutual heading angle (≥ 0.7 rad) are further used. A channel with only one intersection is then used as the first in the string of the ‘W’ shape. Alternatively, an intersection with the highest sum of distances from wall centers is iteratively removed until a wall with one intersection exists. Afterwards, the other wall channels are added to the selected first channel according to the remaining intersections, and if more options exist, by selecting the intersection with shortest distances from wall centers. Finally, the channel centers, lengths, and headings are determined (see Fig. 22b) based on the intersections of the formed ‘W’ shape wall structure.

6. Brick grasping

Brick grasping is the second primary capability for the wall building task. The proposed approach for grasping uses a fusion of color and depth camera sensors for brick detection and visual servoing for precise control during grasping attempts. The grasping state machine is used to govern various stages of grasping with UAV mass and attitude being checked during grasping to abort in case of, e.g., a grasp far from the brick center of mass.

6.1. Brick detection and localization

Brick grasping is based on fast and robust brick detection. A fusion of detections from the color camera and from the depth RealSense sensor is used to improve the robustness. The method of brick detection from the color camera is the same as is used during the scanning (described in Sec. 5.3). Brick detection from the RealSense sensor is similar to the wall detection from the RealSense as described in Sec. 5.2. The altitude of measured points is computed for each pixel of the depth reduced image. Similarly to the wall detection, the brick detection uses altitude thresholding with the threshold value of 0.15 m. Figure 14 shows the result of the thresholding (14c), boundary pixels transformed to UAV coordinate system, and their line approximations (14d - points and dashed lines). The final brick detection is the same as for the color brick detection from Sec. 5.3.

The final data fusion uses a weighted average of the color and depth detections where the weights depend on the quality of the detections. The best quality detection weight 1 is in case of the whole brick contour being visible by the sensor. Supposing

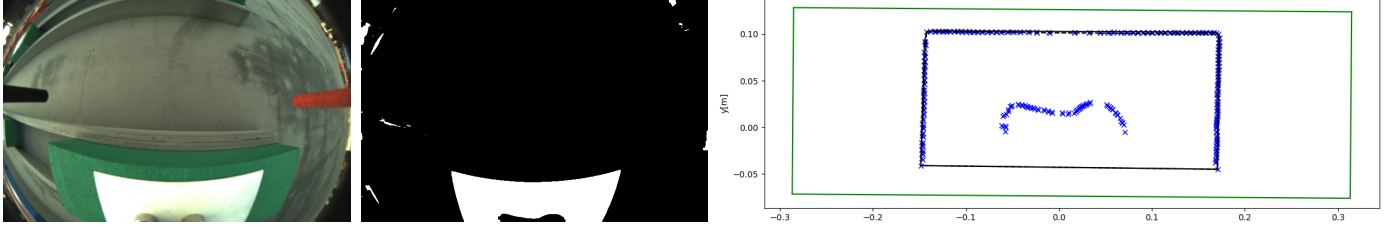


Figure 13: An original image from the color camera, white color segmentation result, and the contours and brick detection results.

three perpendiculars lines represent the contour then the weight 0.5 is used. In case of only two perpendicular lines, the weight 0.25 is used. Example of data fusion is depicted in Fig. 14.

6.2. UAV visual servoing

For precise grasping, we employ a visual servoing technique where the position of the UAV is computed in the coordinate system of the brick that is being grasped. The main challenge of such visual servoing is the ambiguity of the brick's coordinate system (see Fig. 15 with two possible axis placements). The z axis of the brick frame is parallel to the world frame z axis, and therefore the z coordinate is only a shift of the z coordinate in world frame by the brick's height. The brick coordinate system is defined by brick position in world frame \mathbf{b}^W and brick orientation η_b in x, y the axis plane of world frame as seen in Fig. 15. The computation of UAV position within the brick coordinate system must remember the last brick orientation, and thus the choice of initial axis placement. The ambiguity of the brick coordinate system is caused by inaccuracy of brick orientation that can change as the UAV moves closer to the brick.

The detection algorithm finds bricks from actual data in a temporarily created map for data fusion. The last brick orientation is used to select a new brick orientation. The selection is based on the angle difference between orientation of the last brick η_b^{map} and the newly detected brick η_b^{new} . The selection can be expressed as

$$\eta_b = \begin{cases} \eta_b^{new}, & \text{if } \langle \eta_b^{map} - \eta_b^{new} \rangle < \langle \eta_b^{map} - \eta_b^{new} - \Pi \rangle, \\ \eta_b^{new} + \Pi, & \text{otherwise.} \end{cases} \quad (6)$$

The equation uses angle difference $\langle a - b \rangle$ which is the absolute value difference between angle a and angle b , with result in interval $< 0, \Pi >$.

The position of the UAV in world frame system is denoted \mathbf{r}^W . The UAV position \mathbf{r}^O within the coordinate frame O of the brick is expressed as

$$\mathbf{r}^O = \begin{bmatrix} \cos \eta_b & -\sin \eta_b & 0 \\ \sin \eta_b & \cos \eta_b & 0 \\ 0 & 0 & 1 \end{bmatrix} \cdot \begin{bmatrix} \mathbf{r}_x^W - \mathbf{b}_x^W \\ \mathbf{r}_y^W - \mathbf{b}_y^W \\ \mathbf{r}_z^W - 0.2 \end{bmatrix}, \quad (7)$$

where 0.2 represents height of the brick that is used as a shift in the z axis.

6.3. UAV-brick interaction and control

Interaction of a multirotor UAV with the environment is a complex challenge. Small objects, such as the ones being collected during the MBZIRC 2017 challenge [26], posed little to no challenge for common UAVs to carry. However, the much larger and heavier bricks impose torque on the UAV if not grasped in line with the center of mass of the object. Moreover, the grasping event poses a threat to the UAV by possibly limiting the controllable degrees of freedom (DOFs) of the UAV due to mechanical contact.

The first challenge of carrying a sizeable elongated object was solved by designing the underlying UAV control architecture. The control pipeline executes a real-time weight estimator that allows the UAV to not only detect an increase of its weight if an object was grasped, but also to detect a decrease when the UAV rests upon the brick during the grasping maneuver. The estimated mass is used throughout the control pipeline to provide adequate feed-forward control terms and scale the control gains of the employed $SE(3)$ geometric feedback controller [6]. With such measures, our UAVs were able to repeatedly carry all the brick types while performing moderately aggressive maneuvers. It is worth noting our team's UAVs were the smallest vehicles of all teams, which conducted the task autonomously with an approximate 3:1 ratio of UAV mass to brick mass.

The task of grasping a brick requires automatic safety measures to abort the action when the UAV becomes uncontrollable. Such a situation often occurs if the UAV transfers its weight unevenly through its landing gear to the ground during the last moments of the grasping maneuver. This state needs to be detected automatically by measuring the attitude control error and applying acceleration upwards to mitigate the effect quickly. On the other hand, a false positive grasping event can occur when the magnetic gripper fails to attach. This situation is detected as a significant decrease in the estimated mass due to the transfer of the UAV weight thought the gripper to the brick. In both cases, the maneuver is aborted and repeated before a collision can occur.

6.4. Brick grasping state machine

The action of grasping a brick by the UAV was governed by a state machine closely resembling the prize-winning variant from our last success during the MBZIRC 2017 challenge [26]. Figure 16 depicts the states of the grasping state machine. The UAV is expected to be located at the vicinity of the desired brick (such that the brick is visible in the camera) when



Figure 14: Fusion of data for brick detection using color-based (a) and depth-based (b) detection. Thresholded depth data are shown in (c), while the fused data are in (d) showing detections from the color camera as solid line, and from depth camera as dashed line.

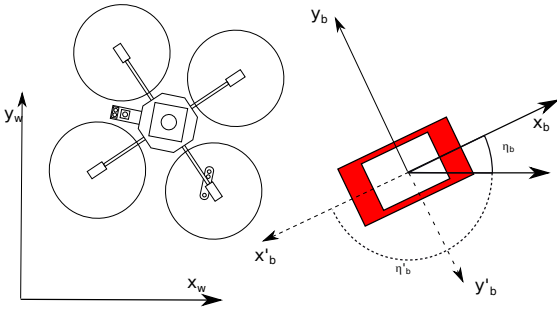


Figure 15: Brick coordinate with two possible axis placements.

the first state is activated. When a brick is detected, the UAV first aligns itself horizontally with the closest brick of the desired color. After the horizontal alignment distance is lower than 0.2 m, the UAV slowly descends to the height of 0.8 m while actively maintaining the alignment. If the alignment is broken, the UAV ascends and attempts to realign with the brick to repeat the process. The process is repeated a maximum of only twice after which the brick is abandoned and its location is temporarily banned to prevent deadlocks. Conversely, when the UAV successfully descends to the height of 0.8 m, it switches its localization system to the direct brick visual servoing (the green states within Fig. 16). The UAV then realigns itself again using only the detected brick as a source of the state estimate. This second alignment starts with 3 cm alignment criterion and relaxes the distance with time. This ensures that the UAV eventually attempts to grasp the brick even if the control accuracy is low. The final grasping maneuver is also performed using the visual localization of the UAV relative to the brick. The process of adaptive and repeated switching from GNSS-based control into visual servoing and back is the main contribution of this part for general object manipulation in demanding outdoor conditions.

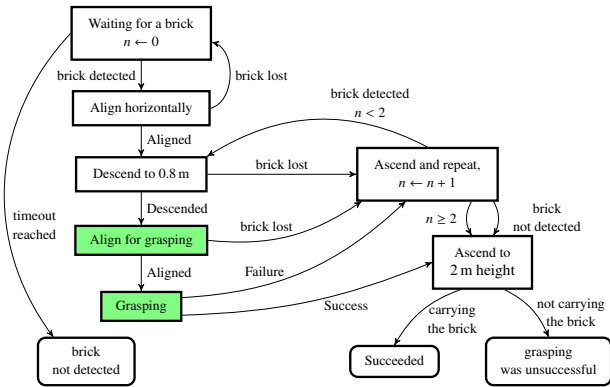


Figure 16: UAV state machine for grasping a particular brick. This whole state machine corresponds to state [S10] within Fig. 6. The white state represents situations when the UAV was localized by the GPS, while in the green state, the states of the UAV were estimated using only the visual detection of the brick for increased precision.

7. Brick placing

7.1. Placing location detection

Place detection uses a similar approach as wall detection (see Sec. 5.2). However, there are three main challenges for detection of locations for where to place the next brick. The top surface of the wall is tiled with a repetitive pattern (see Fig. 17) that makes the stereo camera detection difficult. This problem is solved mainly by filtering minimal distances by reduction of the depth image size. Additionally, the second solution uses a morphological *closing* operation after thresholding. The second challenging aspect is that the view of onboard camera to the wall is partially blocked by the brick attached to the gripper. This problem is solved by applying an automatically created mask after successfully grasping the brick. An example of such a mask is depicted in Fig. 17.

The last challenge is the transparent channel wings that were used to facilitate placement of bricks. These transparent acrylic borders are rather randomly visible on depth measurements and may occasionally appear as a place free for placing a brick. The proposed solution is to detect the free end of the

Algorithm 2: White_plate_detection

Input: I_{thr} – thresholded image**Output:** (x, y, α) — center of the white plate with α plate rotation

```
 $I_{clo} = \text{morphology\_close}(I_{thr})$  // OpenCV functions
erode, dilate
Contours = findContours( $I_{clo}$ ) // OpenCV functions
findContours
for Contour  $\in$  Contours do
  Points =  $\emptyset$ 
  for  $p \in$  Contour do
     $v = \text{undistort}(p)$  //  $v$  is vector pointing in
    undistorted direction
     $v' = R \cdot v$  //  $R$  is the rotation matrix from
    sensor to world frame
     $coef = UAV_{pos}(2) - \text{brick\_height}$  //  $UAV_{pos}(2)$ 
    is altitude of the UAV
     $p' = UAV_{pos} + v' \cdot coef$ 
    Add  $p'$  into list Points
  Convex = convexHull(Points) // OpenCV functions
  convexHull
  if Contour is not at border then
    box = minAreaRect(Convex) // OpenCV
    functions minAreaRect
    if box has correct size then
      output  $(x, y, \alpha)$  –  $(x, y)$  is box
      center,  $\alpha$  — is box
      orientation
  else
    Lines = approxPolyDP(Convex) // only for
    detection from distance less than 1.5 m
    if Lines forms U shape and size of U shape is
    correct then
      find middle parallel line inside U shape and
      found expected brick center  $(x, y)$ 
      output  $(x, y, \alpha)$  —  $\alpha$  — is middle line
      orientation
```

wall by detecting the leftmost border point of the thresholded image (see Fig. 18).

The method for detecting the placing spot on the wall assumes the wall segment is already aligned with the wider axis of the camera image. The alignment is initially governed by the global planner which operates with necessary information obtained during the initial sweep. The size of the brick being placed is known since the grasping procedure, and thus the method detects a place on the free wall at a correct distance from the leftmost border of the detected wall segment within the image. As two layers of bricks can be built on the wall, the free area on the wall depends on the currently active layer. In many cases, such free space contains a transparent acrylic border of the wall. This border is removed from the detected wall by morphological *erosion*.

The leftmost place on the wall is selected and if the left border of the wall is not visible, the UAV moves to the leftmost part of a visible wall to find the correct edge. The results of this algorithm are depicted in Fig. 18.

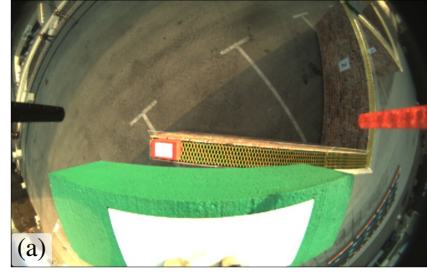


Figure 17: Original data from the color camera (a) and original depth data (b). The mask (c) for the depth data is used to remove the carried brick and the UAV leg in the top part of the mask.

7.2. Placing state machine

The action of placing a brick on the wall is governed by the state machine depicted in Fig. 19. This lower-level state machine is responsible for guiding the UAV above the spot designated for placement and controlling the descent to a desired height above the wall. Since the outcome of placing a brick can rarely be influenced after releasing the brick from the magnetic gripper, we do not consider any actions in case of failure. Moreover, numerous bricks are available in the grasping area, so grasping a misplaced brick or even repairing the wall is forfeit over continuing for a fresh brick. Therefore, the placing state machine sequentially follows the actions of aligning horizontally with the wall and descending while aiming for the designated spot. If anything fails, the held brick is dropped and the UAV continues above the brick area to obtain a new brick. This was chosen so as to not counteract any potential failure states, such as sudden misalignment (e.g., caused by localization drift). A simpler yet capable approach was chosen due to the added complexity and less-deterministic execution of a more failure-proof solution.

8. Experimental results

This section describes the results achieved during the MBZIRC Challenge 2 competition trials using the proposed system. The herein system for wall building by UAVs, developed as detailed above by the CTU-UPenn-NYU team, was able to win Challenge 2 by placing the far most number of bricks, mostly with the UAVs. However, the UGV deployed in the challenge also contributed by autonomously placing a brick during the second competition trial as described in [43]. The CTU-UPenn-NYU team won by scoring 8.24 points, while the second Nimbro Team (University of Bonn) scored 1.33 points, and the third (Technical University of Denmark) 0.89 points. Figure 26 depicts the team at the winner stand.

Prior to the competition, the team dedicated over a month for preparation and experimental evaluation in a desert near

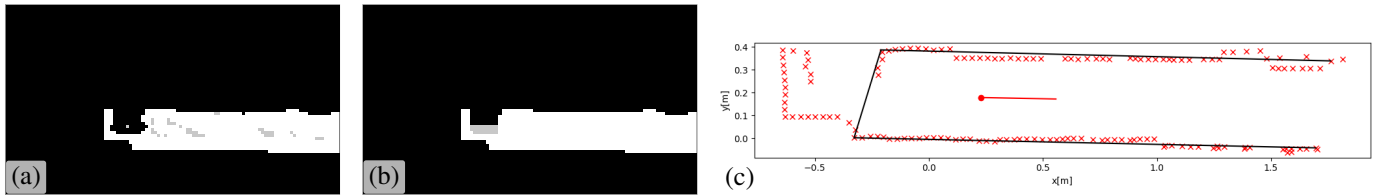


Figure 18: Thresholded depth data (a) and thresholded data after applying the morphological *closing* operation (b). The result of place detection (c) where the red line demonstrates shift from the center of the wall to the leftmost position of the brick.

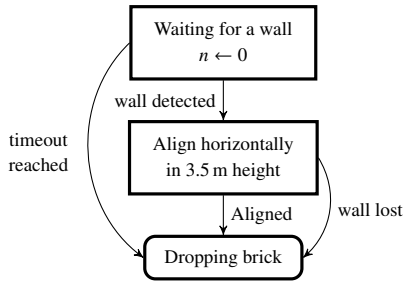


Figure 19: UAV state machine for placing a brick on the wall. This state machine corresponds to state [S12] within Fig. 6.

Abu Dhabi. Real world experiments could not be conducted in the Czech Republic in the final months of preparations due to the winter weather conditions. Therefore, the team decided to conduct final preparation near the competition venue, despite the unforgiving high temperatures, sand, and wind conditions of the coastal United Arab Emirates. This preparation phase proved to be crucial in securing first place in the competition just as it was in 2017. Figure 20 depicts photos from the desert experiments. Videos from the experiments are available at <http://mrs.felk.cvut.cz/mbzirc-2020-uav-wall>.

Table 2 shows the overall performance of the system during the two competition trials, each lasting 25 minutes. It shows the types of bricks, denoted as ‘R’ for RED and ‘G’ for GREEN, in the order they were grasped during the individual trials. The grasping of BLUE bricks was not attempted during the competition trials, although the UAVs were capable of carrying them, mainly due a significantly higher detachment probability of a grasped brick caused by the pendulum effect of the longer and heavier BLUE brick. The grasping of ORANGE bricks was also not attempted for similar reasons and difficulty of cooperative carrying. The competition did not require delivering any ORANGE bricks to qualify for obtaining points. The grasped bricks are further displayed per individual restarts within the trials, where the restart had the possibility of keeping the already placed bricks and running the system again with all robots in their initial positions.

Table 2 shows all grasped bricks, although not all were successfully placed on a wall. The bricks denoted with ‘*b*’ index did not have successful placement, which in most cases was due to the brick bouncing off the wall after release. The single case of a placed RED brick during the fourth restart of the first trial, denoted with ‘*s*’ index, is a placement into the second layer of

Table 2: Grasped bricks during the two competition trials of Challenge 2.

Trial	Restart	UAV1	UAV3
one	1	R ^{<i>b</i>} , R, G, G ^{<i>b</i>}	G
	2	R, R, G ^{<i>b</i>}	R, G ^{<i>b</i>}
	3	R ^{<i>b</i>} , R ^{<i>b</i>}	R, R
	4	G	R ^{<i>s</i>} , R ^{<i>b</i>}
two	1	G, G, R ^{<i>b</i>} , R ^{<i>b</i>} , R	–

a particular channel which was also not achieved by any other team.

Notice that only UAV1 and UAV3 were used for wall building during the competition trials. The strategy of having UAV2 wait for a collision or battery depletion of another UAV was not required during the competition. However, this reliable multi-UAV strategy was successfully tested during the pre-competition trials.

Ten bricks were successfully placed on the wall during the first trial consisting of seven RED and three GREEN bricks. Seven bricks bounced off the wall during the same trial. The main focus of the CTU-UPenn-NYU team during the second trial was to autonomously place at least one brick using the UGV as was required for winning the challenge. Therefore, many restarts were done to ensure this goal and only before the first restart were the UAVs used to grasp and place bricks as shown in Table 2. In the rest of this section, we focus on the individual (i.e. scanning, grasping, placing) wall building sub-tasks and the overall performance achieved during the first trial, in which UAVs were used throughout the entire trial.

8.1. Scanning for bricks and wall placement

Scanning of the arena was the first subtask of the proposed UAV wall building approach performed in order to find the location of the brick stack and wall position designed for the UAVs. The arena scanning was planned using a zig-zag path within the predefined arena space (defined by arena corners and safety area) as described in Sec. 5.1.

Figure 21 shows all brick detections (RED, GREEN and BLUE- ORANGE bricks were not considered) as well as the detections of the wall channels. The zig-zag scanning path is shown within the arena boundaries as recorded by the onboard GPS. The employed brick detection using the onboard RGB camera was able to detect bricks in the range of $\approx 10\text{ m} \times 5\text{ m}$



Figure 20: Photos from preparation in the Abu Dhabi desert. Videos are available at <http://mrs.felk.cvut.cz/mbzirc-2020-uav-wall>.

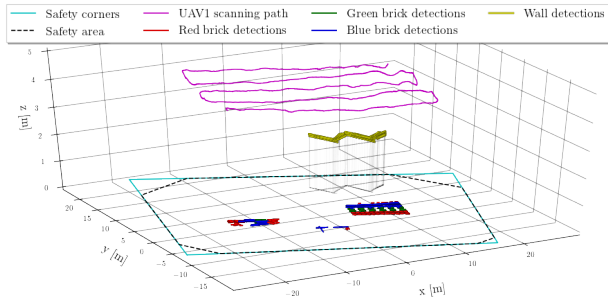


Figure 21: Path of UAV1 while scanning the arena and detections of the bricks and UAV wall channels.

in $x \times y$ coordinates of the camera when flying at the scanning 4.5 m height. However, robust detections of bricks were obtained in range of $\approx 5 \text{ m} \times 3 \text{ m}$ of $x \times y$ coordinates. This required an overlapping camera field of view while following the zig-zag pattern path.

Figure 21 clearly shows the ‘W’ letter shape of the four wall channels created by the wall detections. The brick detections form two large clusters being the UGV and UAV brick stacks. The UAV stack being wider was further used for the PCA analysis. Figure 21 also features a set of false positive brick detections between the two brick stacks corresponding to the position of waiting UAV2 and the starting takeoff area marked as a white rectangle on the ground.

After completion of the scanning path, the wall and brick detections are processed to create a topological map of the arena. The map contains positions of the individual wall channels ordered in a ‘W’ letter chain as well as lines along the particular brick types that can be deterministically divided among the three UAVs. Figure 22 shows the brick and wall detections already filtered out by the number of reoccurrences during the scanning. Figure Fig. 22a shows all the wall detections and the two bricks GMM clusters with corresponding PCA component variances proportional to width and height of the two brick stacks. Figure Fig. 22b features only the UAV stack together with the topological map consisting of ‘wall 0’–‘wall 3’ and the red and green brick lines. The positions of the mapped walls and brick lines are then shared among UAVs and used to distribute the wall building task, as was detailed before in Sec. 4.2.

By comparing Fig. 21 and Fig. 22, it can be seen that the initial reoccurrences-based filter removes the false positive de-

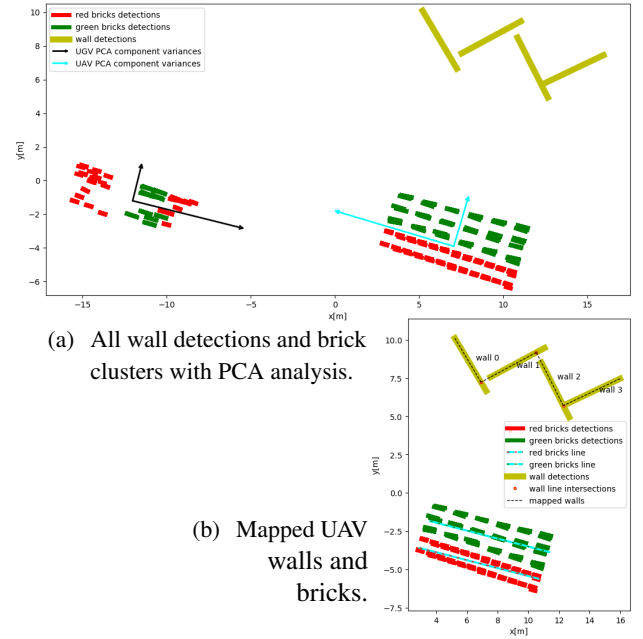


Figure 22: Topological map based on scanning of the arena.

tectations present in the takeoff area. However, the blue bricks present in the Fig. 21 are also filtered out and are instead incorrectly labeled as green bricks in most detections. The PCA analysis indeed selects the correct brick stack for UAVs having the larger width, with the smaller variance component being larger for the UAV stack. Figure 22b shows that the wall detections are correctly recognized as ‘wall 0’–‘wall 3’ based on the intersections of line approximations of the wall detections. Moreover, the wall detection and mapping shows a great performance by creating the individual channels of almost the same size based only on the detections and analysis of the intersections. Finally, by comparing the raw wall detections and the mapped walls, we can see a *shadow effect* of the wall detection in 1.7 m when projected to the ground plane due to the left-to-right scanning trajectory above the wall.

8.2. Brick grasping

The brick grasping is another key capability required for competing in the wall building task. The grasping procedure [S10] consists of the lower-level grasping state machine described in Sec. 6.4. Figure 23 shows the evolution of the grasping states with respect to the UAV position for the first success-

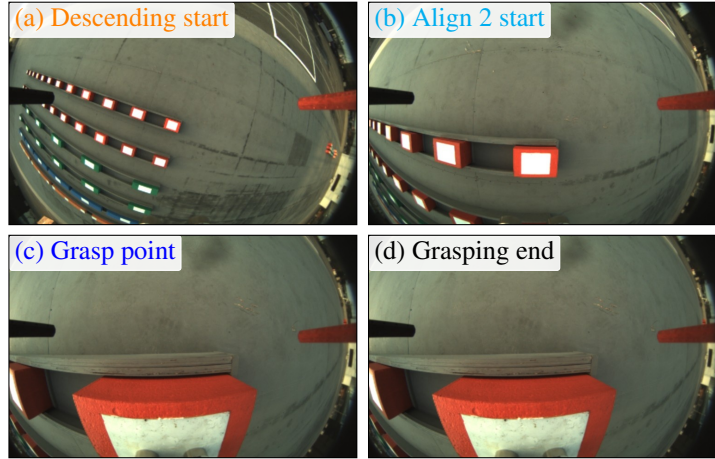
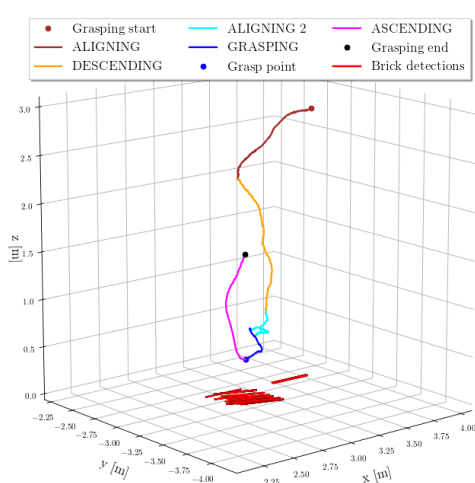


Figure 23: Grasping of a red brick with color indicated stages of the grasping procedure.

ful grasp of the red brick with UAV1 during the second restart of first trial.

Figure 23 also features the images taken by the mvBlueFOX camera that used for RGB detection of the bricks during various stages of the grasping state machine. The brick detections are shown as measured during the grasping. The rest of the detections have a mean position for x , y , heading being 3.022 m, -3.215 m, 2.825 rad, respectively, and a corresponding standard deviation of 0.029 m, 0.077 m, 0.077 rad, respectively. However, the absolute localization of the grasped brick is only relevant within the first two stages of the grasping manoeuvre (the first alignment and descent), where the UAV is guided using these estimated GPS coordinates of the brick. The later stages use direct visual servoing to estimate the UAV states using the brick detections which outperforms the accuracy of standard GPS by an order of magnitude. Our UAVs were able to target the magnetic plates on the bricks reliably within centimeter precision.

8.3. Brick placement

Brick placement together with grasping is one of the most important wall building capabilities. Figure 24 depicts the successful placement of the same brick being grasped in Fig. 23. After successful grasping, the UAV flies above its assigned wall channel and switches to the lower-level placement state machine using place detection (both described in Sec. 7) to guide the UAV above the release point on the appropriate location of the wall. Note that the pattern (i.e. sequence of bricks in both layers) forming individual channels was given for each trial. The brick building sequence was planned as a consecutive placement of a brick into the next unoccupied position in the wall segment — either the leftmost position in the completely-free segment or neighbouring position to the rightmost brick on the segment. Figure 24 shows the stages of the lower-level placement state machine together with the UAV positions and detections of the wall channel during alignment and placing states. Additionally, the images from both the RGB mvBlueFOX camera and the depth images from the RealSense camera are shown in various stages of placement.

In Fig. 24, it can be seen that placement starts at approximately the middle of the assigned wall channel. During the alignment state, the UAV moves along the channel to the leftmost position on the empty wall. The wall detections are clearly shown to be of various lengths as the smaller portion of the wall is visible once descending during the placing state. However, the left corner of the wall is measured during the detections with a mean position for x , y , heading being 5.374 m, 9.790 m, -1.110 rad, respectively, with corresponding standard deviation of 0.139 m, 0.093 m, 0.113 rad, respectively.

The brick placing state machine is comparably simpler than the grasping state machine, since the grasping state machine needs to cover various failure stages during the grasping process. This was required to deal with failures in the grasping stage, because the UAV adds no value to the mission outcome if it does not succeed with grasping. Moreover, the grasping manoeuvre is sensitive to control accuracy and timing while also being more dangerous for the UAV. On the other hand, placing allows for a significant slack in the control of the UAV thanks to the width of the wall channel and the possibility of dropping the brick from a higher height without any physical interaction with the wall. The wall detection also worked more reliably thanks to more prominent features in sensory input as the UAV rarely lost the wall from its field of vision during testing. Lastly, we did not consider any possible correcting action for instances of improperly placed bricks.

8.4. Wall building performance

Finally, the performance of the wall building stage using the proposed system is depicted in Fig. 25 showing the recorded positions of both the UAV1 and UAV3 throughout the first trial with four performed restarts. All 17 grasped bricks are shown with their respective release positions, however only ten bricks stayed on the wall without bouncing off as detailed in Table 2. The recorded positions of the UAVs shown do not include the initial scanning of UAV1 already discussed in the Sec. 8.1. Instead, the positions of the UAVs once carrying bricks is highlighted. The mapped wall and brick locations are based on the

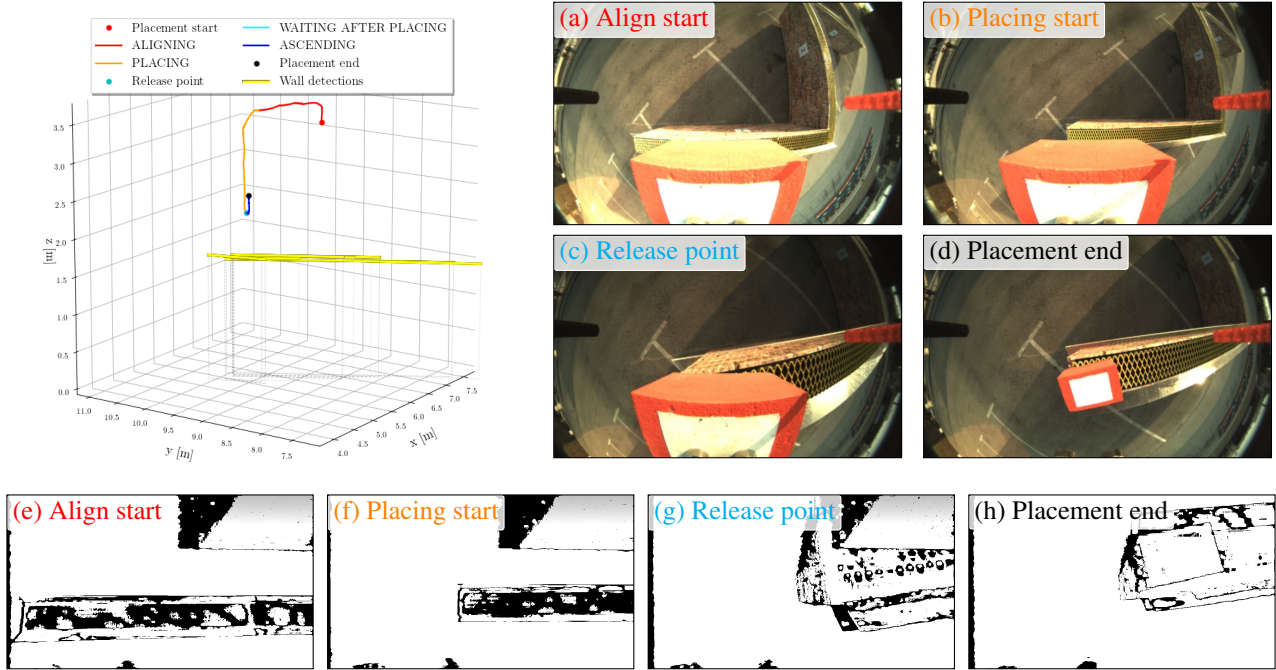


Figure 24: Placement of a red brick on the beginning of the first wall channel shown with placement stages and wall detections, together with images from the RGB camera (a)–(d) and depth camera (e)–(h). Videos from experimental testing and from the competition are available at <http://mrs.felk.cvut.cz/mbzirc-2020-uav-wall>.

scanning in the second restart as already shown in Fig. 21 and Fig. 22.

See video of the CTU-UPenn-NYU team <https://youtu.be/1-aRtSarYz4> with summary of the preparations in the Abu Dhabi desert, of competition rehearsals, and of the actual Challenge 2 MBZIRC 2020 competition trials.

8.5. Lessons learned

The most important factor driving development was the need for safety and reliability of the multi-UAV system. Interaction with the environment during grasping and placing is potentially dangerous and can easily damage the UAV. The use of real-time weight and force estimation for the detection of potentially dangerous situations was of significant benefit. A common approach of relying solely on UAV position estimation to drive the decision-making process would not be sufficient.

One of the tunable parameters of the grasping/placing maneuvers was the speed of the descent. Speed too slow increases the overall duration of the UAV being in a potentially dangerous location and allows the ground effect to build up (aerodynamic effects caused by the rotor downwash close to a ground). Alternatively, too fast of speed increases the risk of damaging the UAV due to the sudden bump caused by interaction with the brick, the wall, or the ground. On several occasions during our preparations, we experienced a complete stall of motors due to the sudden impact at higher speed, which subsequently caused a loss of onboard power and an uncontrollable, unstoppable tumbling of the UAV. Therefore, we advise caution when working with UAVs if sharp acceleration spikes may be transmitted to

the UAV body. Finally, we settled on the descending speed of 0.25 m s^{-1} which showed to be the most reliable and rewarding.

This proposed wall building system depends on successful arena scanning and creation of a topological map used for planning further brick pickup and placement. As such, the brick and wall detections need to be robust and without excessive false positives that could influence the topological map creation based on statistical analysis of detections. The task was further challenging due to the stack of UGV bricks present that could not be used safely by UAVs and thus had to be recognized among the detections. During the preparations, a rather high number of false detections forced implementing significant detection filtering during scanning, requiring a minimal number of corrections in the detection map and used the iterative median filtering of detections to remove outliers. However, during the competition rehearsals, the creation of the topological map had to be further fine-tuned to, e.g., filter out already placed bricks from previous restarts.

Finally, the GPS drift significantly influenced the entire system deployment as arena borders were defined in GPS coordinates, with either the brick stack or the wall channels possibly placed too close to the borders. This prevented UAVs from flying too close to the net-protected borders and suggests that an additional LiDAR or camera-based detection of the border (or even sensor-based fix of the GPS drift) would significantly improve deployment robustness in similar competitions. An RTK-based localization is technically a possible solution to this problem, but it was not used by the team due to the penalization of RTK in scoring. However, after discussion with potential industrial partners, a solution using both the RTK GPS and the

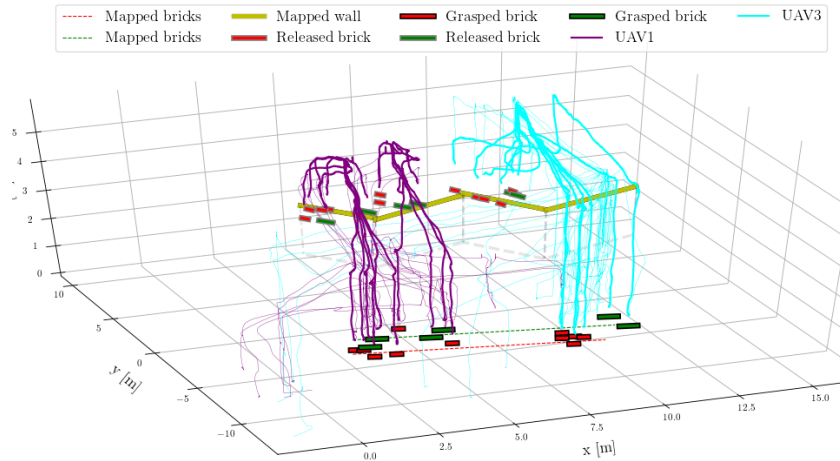


Figure 25: Visualization of wall building performance during the first trial with shown grasping/placing positions and highlighted UAV trajectories by the thicker lines when carrying a brick.

onboard local sensors would be preferred. Important construction locations could be pre-measured using the RTK (as it is nowadays common on construction sites). Combining this with the proposed onboard sensor capabilities would yield a robust cognitive system capable of reacting to changes in the environment.

The execution time of brick detection for visual servoing is critical for smooth real-time UAV control and navigation. The Intel NUC computer, by its design similar to laptop hardware, had a power-saving mode that caused irregular execution times of our methods. This problem was detected before the competition and resolving it improved the robustness of the whole system significantly.

9. Conclusions

In this paper, an autonomous system developed by CTU-UPenn-NYU team for wall building with a team of UAVs was introduced. The examined task was part of Challenge 2 of the MBZIRC 2020 where three UAVs were assigned to find, pickup, and place color-typed bricks on a prepared wall structure. The goal of the task was to maximize collected points for placing the bricks while following the prescribed wall pattern. This paper presents the key parts of the UAV system developed for the competition, including the UAV control system, the algorithms for brick and wall detection, the single robot state machine, and the multi-robot distributed approach for the task. The core autonomous capabilities of scanning the arena for wall/brick locations, autonomous grasping using visual servoing technique, and precise placement of bricks on the wall structure are described in detail. We further report the experimental results achieved during the competition trials showing the performance of the core autonomous capabilities and of the entire system. The proposed approach performed the best among all participants with 22 successfully grasped bricks in which 13 of these bricks were successfully placed during the



Figure 26: CTU-UPenn-NYU team after winning the wall building Challenge 2 of MBZIRC 2020.

two trials of the Challenge 2 MBZIRC competition. The entire system for the wall building task is open-sourced for the community to be used for possible deployment and future development. It can also serve as a useful reference for future robotic challenges, such as the MBZIRC that indeed serves as a great verification of robotic research.

Acknowledgements

We thank the University of Pennsylvania and the New York University for the collaboration as the members of the CTU-UPenn-NYU team (see Fig. 26). This work would not have been possible without the tireless dedication of all the team members and support and patience from their families. The presented work has been supported by Khalifa University and by CTU grant no. SGS20/174/OHK3/3T/13.

References

- [1] M. C. Tatum, J. Liu, Unmanned aircraft system applications in construction, *Procedia Engineering* 196 (2017) 167–175.
- [2] Y. Ham, K. K. Han, J. J. Lin, M. Golparvar-Fard, Visual monitoring of civil infrastructure systems via camera-equipped Unmanned Aerial Vehicles (UAVs): a review of related works 4 (1) (2016) 1–8.

- [3] J. Howard, V. Murashov, C. M. Branche, Unmanned aerial vehicles in construction and worker safety, *American Journal of Industrial Medicine* 61 (1) (2018) 3–10. doi:10.1002/ajim.22782.
- [4] Khalifa University, Mohamed bin zayed international robotics challenge 2020, available online, <https://www.mbzirc.com/challenge/2020>, accessed on, cited on 2020/11/16.
- [5] T. Baca, D. Hert, et al., Model Predictive Trajectory Tracking and Collision Avoidance for Reliable Outdoor Deployment of Unmanned Aerial Vehicles, in: 2018 IEEE/RSJ IROS, IEEE, 2018, pp. 1–8.
- [6] T. Lee, M. Leoky, et al., Geometric tracking control of a quadrotor UAV on SE(3), in: 2010 IEEE CDC, IEEE, 2010, pp. 5420–5425.
- [7] T. Baca, M. Petrlík, M. Vrba, V. Spurný, R. Penicka, D. Hert, M. Saska, The MRS UAV System: Pushing the Frontiers of Reproducible Research, Real-world Deployment, and Education with Autonomous Unmanned Aerial Vehicles, submitted to JINT (8 2020). arXiv:2008.08050v2.
- [8] J. Zink, B. Lovelace, Unmanned aerial vehicle bridge inspection demonstration project, Tech. rep. (2015).
- [9] Q. Lindsey, D. Mellinger, V. Kumar, Construction of cubic structures with quadrotor teams, *Proc. Robotics: Science & Systems VII* (2011).
- [10] Q. Lindsey, et al., Distributed construction of truss structures, in: *Algorithmic Foundations of Robotics X*, Springer, 2013, pp. 209–225.
- [11] F. Augugliaro, A. Mirjan, et al., Building tensile structures with flying machines, in: 2013 IEEE/RSJ IROS, IEEE, 2013, pp. 3487–3492.
- [12] A. Mirjan, F. Augugliaro, R. D’Andrea, F. Gramazio, M. Kohler, Building a bridge with flying robots, in: *Robotic Fabrication in Architecture, Art and Design 2016*, Springer, 2016, pp. 34–47.
- [13] D. Alejo, J. A. Cobano, et al., Collision-Free 4D Trajectory Planning in Unmanned Aerial Vehicles for Assembly and Structure Construction, *Journal of Intelligent & Robotic Systems* 73 (1) (2014) 783–795.
- [14] F. Augugliaro, S. Lupashin, M. Hamer, C. Male, M. Hehn, M. W. Mueller, J. S. Willmann, et al., The flight assembled architecture installation: Cooperative construction with flying machines, *IEEE Control Systems Magazine* 34 (4) (2014) 46–64.
- [15] Aerial Robotics Cooperative Assembly system, retrieved from <http://www.arcas-project.eu>, 2020/08/28 (2020).
- [16] F. Ruggiero, V. Lippiello, A. Ollero, Aerial manipulation: A literature review, *IEEE Robotics and Automation Letters* 3 (3) (2018) 1957–1964.
- [17] K. Kondak, K. Krieger, A. Albu-Schaeffer, M. Schwarzbach, M. Laiacker, I. Maza, et al., Closed-Loop Behavior of an Autonomous Helicopter Equipped with a Robotic Arm for Aerial Manipulation Tasks, *International Journal of Advanced Robotic Systems* 10 (2) (2013) 145–154.
- [18] K. Kondak, F. Huber, M. Schwarzbach, M. Laiacker, et al., Aerial manipulation robot composed of an autonomous helicopter and a 7 degrees of freedom industrial manipulator, in: 2014 IEEE ICRA, IEEE, 2014, pp. 2107–2112.
- [19] M. Ryll, G. Muscio, F. Pierri, E. Cataldi, G. Antonelli, F. Caccavale, A. Franchi, 6D physical interaction with a fully actuated aerial robot, in: 2017 IEEE ICRA, IEEE, 2017, pp. 5190–5195.
- [20] J. Munoz-Morera, I. Maza, C. J. Fernandez-Aguera, F. Caballero, A. Ollero, Assembly planning for the construction of structures with multiple UAS equipped with robotic arms, in: 2015 IEEE ICUAS, IEEE, 2015, pp. 1049–1058.
- [21] J. Thomas, G. Loianno, et al., Toward image based visual servoing for aerial grasping and perching, in: 2014 IEEE ICRA, IEEE, 2014, pp. 2113–2118.
- [22] P. Ramon Soria, B. C. Arrue, A. Ollero, Detection, location and grasping objects using a stereo sensor on UAV in outdoor environments, *Sensors* 17 (1) (2017) 103.
- [23] A. Gawel, M. Kamel, T. Novkovic, J. Widauer, D. Schindler, B. P. Von Altschhofen, R. Siegwart, J. Nieto, Aerial picking and delivery of magnetic objects with MAVs, in: 2017 IEEE ICRA, IEEE, 2017, pp. 5746–5752.
- [24] K. Feng, W. Li, S. Ge, F. Pan, Packages delivery based on marker detection for UAVs, in: 2020 IEEE CCDC, IEEE, 2020, pp. 2094–2099.
- [25] G. Loianno, V. Spurný, J. Thomas, T. Baca, D. Thakur, D. Hert, R. Penicka, T. Krajník, A. Zhou, A. Cho, M. Saska, et al., Localization, Grasping, and Transportation of Magnetic Objects by a team of MAVs in Challenging Desert like Environments, *IEEE Robotics and Automation Letters* 3 (3) (2018) 1576–1583.
- [26] V. Spurný, T. Baca, M. Saska, R. Penicka, T. Krajník, J. Thomas, D. Thakur, G. Loianno, et al., Cooperative Autonomous Search, Grasping and Delivering in a Treasure Hunt Scenario by a Team of UAVs, *Journal of Field Robotics* 36 (1) (2019) 125–148.
- [27] A. R. Castano, F. Real, P. Ramon-Soria, J. Capitan, V. Vega, B. C. Arrue, et al., AI-Robotics team: A cooperative multi-unmanned aerial vehicle approach for the Mohamed Bin Zayed International Robotic Challenge, *Journal of Field Robotics* 36 (1) (2019) 104–124.
- [28] NicaDrone, Electro Permanent Magnet OpenGrab EPM V3, retrieved August 22, 2020, from <https://nicadrone.com/products/epm-v3> (2020).
- [29] R. Bahnemann, M. Pantic, M. Popovic, D. Schindler, M. Tranzatto, M. Kamel, M. Grimm, J. Widauer, R. Siegwart, J. Nieto, The ETH-MAV Team in the MBZ International Robotics Challenge, *Journal of Field Robotics* 36 (1) (2019) 78–103.
- [30] M. Kamel, J. Alonso-Mora, R. Siegwart, J. Nieto, Robust Collision Avoidance for Multiple Micro Aerial Vehicles Using Nonlinear Model Predictive Control, in: 2017 IEEE/RSJ IROS, IEEE, 2017, pp. 236–243.
- [31] M. Beul, M. Nieuwenhuisen, J. Quenzel, R. A. Rosu, J. Horn, D. Pavlichenko, S. Houben, S. Behnke, Team NimbRo at MBZIRC 2017: Fast landing on a moving target and treasure hunting with a team of micro aerial vehicles, *Journal of Field Robotics* 36 (1) (2019) 204–229.
- [32] M. Beul, S. Behnke, Fast full state trajectory generation for multirotors, in: 2017 IEEE ICUAS, IEEE, 2017, pp. 408–416.
- [33] Open Robotics, Robotic Operating System, retrieved July 22, 2020, from <https://www.ros.org> (2020).
- [34] P. Schillinger, S. Kohlbrecher, O. von Stryk, Human-robot collaborative high-level control with application to rescue robotics, in: 2016 IEEE ICRA, IEEE, 2016, pp. 2796–2802.
- [35] J. Bohren, S. Cousins, The smach high-level executive [ros news], *IEEE Robotics Automation Magazine* 17 (4) (2010) 18–20.
- [36] M. Schwarz, nimbros_network - ros transport for high-latency, low-quality networks, available online, https://github.com/AIS-Bonn/nimbros_network, accessed on 2020/11/16.
- [37] E. Galceran, M. Carreras, A survey on coverage path planning for robotics, *Robotics and Autonomous Systems* 61 (12) (2013) 1258–1276.
- [38] A. Grunnet-Jepsen, J. N. Sweetser, J. Woodfill, Best-Known-Methods for Tuning Intel® RealSense™ D400 Depth Cameras for Best Performance, Tech. rep., Intel Corporation: Santa Clara, CA, USA (2018).
- [39] G. Bradski, The OpenCV Library, *Dr. Dobbs’ Journal of Software Tools* (2000).
- [40] D. Scaramuzza, A. Martinelli, R. Siegwart, A toolbox for easily calibrating omnidirectional cameras, in: 2006 IEEE/RSJ IROS, IEEE, 2006, pp. 5695–5701.
- [41] D. Reynolds, Gaussian mixture models, *Encyclopedia of Biometrics* 741 (2009) 659–663.
- [42] I. Jolliffe, *Principal Component Analysis*, 2011, pp. 1094–1096.
- [43] P. Stibinger, G. Broughton, F. Majer, Z. Rozsypalek, A. Wang, K. Jindal, A. Zhou, D. Thakur, G. Loianno, T. Krajník, M. Saska, Mobile Manipulator for Autonomous Localization, Grasping and Precise Placement of Construction Material in a Semi-structured Environment, Submitted to *Robotics and Automation Letters* (2020). arXiv:2011.07972.